Report No. CG-D-1-86

ADVANCED PROPULSOR DESIGN STUDIES

BY

WALTER S. GEARHART

FINAL REPORT

JUNE 1985

AD-A164 983

DTIC FILE COPY

DTIC
ELECTE
MAR 4 1986
S D
B

86 3 4 057

## NOTICE

| 1. Report No. CG-D-1-86 | 2. Government Accession No. AD-A164983 | 3. Recipient's Catalog No. |
|---|---|---|

| 4. Title and Subtitle | 5. Report Date June 1985 |
|---|---|
| Advanced Propulsor Design Studies | 6. Performing Organization Code |
| | 8. Performing Organization Report No. |

| 7. Author's) Walter S. Gearhart | |
|---|---|

| 9. Performing Organization Name and Address Pennsylvania State University Applied Research Laboratory State College, Pennsylvania 16804 | 10. Work Unit No. (TRAIS) |
|---|---|
| | 11. Contract or Grant No. DTCG23-84-F-20046 |

| 12. Sponsoring Agency Name and Address United States Coast Guard (G-DMT/54) 2100 Second Street, S. W. Washington, D. C. 20593 | 13. Type of Report and Period Covered Final Report |
|---|---|
| | 14. Sponsoring Agency Code U. S. Coast Guard Headquarters |

15. Supplementary Notes

16. Abstract

Various propulsor configurations are studied on a preliminary design basis to determine their relative performance when operating on two different United States Coast Guard (USCG) boats. On the basis of these studies a detailed design of an advanced propulsor arrangement was performed for application on a USCG 41' utility boat. Full scale test results for the Advanced Propulsor on the 41' UTB shall be in a follow-on report.

| 17. Key Words Pre-swirl vanes Vanes Propeller Energy Conservation | 18. Distribution Statement This document is available to the U. S. Public through the National Technical Information Service Springfield, VA 22161 |
|---|---|

| 19. Security Classif. (of this report) Not Classified | 20. Security Classif. (of this page) Not Classified | 21. No. of Pages 55 | 22. Price |
|---|---|---|---|

Form DOT F 1700.7 (8-72)          Reproduction of completed page authorized

# Table of Contents

## List of Tables

DTIC
ELECTE
MAR 4 1986
B

Accession For

NTIS GRA&I
DTIC TAB
Unannounced
Justification

By
Distribution/

Availability Codes

Dist | Avail and/or Special

A-1

QUALITY INSPECTED 3

## List of Figures

List of Figures (Cont'd)

Nomenclature

$\rho$        mass density

$Q$        volumetric flow-rate through propulsor

$\Delta V$        change in axial velocity through propulsor

$\overline{V_1}$        mass averaged velocity upstream of propulsor

$V_\infty$        ship speed

$V_\theta$        tangential velocity

$V_a$, $V_R$        axial velocity

$A_B$        reference area

$\eta_p$        propulsive efficiency (Equation 2a)

$\eta_H$        hydraulic efficiency (Equation 6a)

$\eta_D$        $(\eta_P)(\eta_H)$

$A_1$        area associated with the ingested flow at a station upstream of propulsor

$r_h$        hull or hub radius

$r_B$        reference radius

$p$        static pressure

$J_P$        advance ratio based on propeller diameter and ship speed

$r_T$        tip radius of rotor blades

$C_D$          drag coefficient of ship (defined in Table I)

$C_m$         mass flowrate coefficient

$C_T$          thrust coefficient (Equation 1a)

$K_X$         nondimensional force applied to ship in direction of ship motion

$D_P$          propeller diameter

$W$           velocity relative to rotor blade

$C_D$         $\dfrac{\text{Resistance}}{\rho \dfrac{V_\infty^2}{2} A_{Ref}}$

$C_P$         $\dfrac{\text{Shaft Power}}{\rho \dfrac{V_\infty^3}{2} A_{Ref}}$

$A_{Ref}$      reference area based on propeller diameter

$D_{Ref}; D_P$    propeller diameter

$r$            radial distance from axis of rotation

$N$          number of blades

## Introduction

It is the purpose of the propulsor to convert rotational shaft energy into a propulsive thrust. Ideally, this conversion is to be accomplished with the most efficient, vibration-free and inexpensive device. However, emphasis on achieving a particular performance goal such as cavitation resistance, efficiency, or propulsor weight and mechanical simplicity may limit the designer in the type of propulsor configuration to be selected. It is the intent of this document to review the propulsive characteristics of various propulsor types for application on planing hull type craft. On the basis of these studies the performance advantages and shortcomings associated with each type of propulsor will be discussed.

The performance of the conventional open propeller as well as propellers employing stationary counterswirl vanes located upstream of the propeller (reaction fin propulsor) shall be reviewed. Ducted propulsors employing a stator blade located upstream of the rotor shall also be considered. *Keywords: pre-swirl vanes; energy conservation, Coast Guard ships; charts.*

The most common and simplest propulsor that has been applied is the standard open propeller. A propeller operating in water experiences energy losses by two mechanisms. There are frictional losses as the blades pass through the fluid. An efficiency loss also occurs because energy is transferred to the fluid by the blading and is lost in the slipstream.

Power losses associated with frictional effects on a rotating blade are approximately proportional to the cube of the blade-surface velocity and the wetted surface area of the propeller. To reduce frictional losses the propeller should be small in diameter and have a minimum number of blades of small chord. The frictional losses are also reduced if the propulsor is designed to have a relatively high advance coefficient (ratio of ship speed to tip velocity of propeller blades). The blade-surface velocity will then be reduced to a value approaching the forward speed of the ship.

1

Reduction of frictional losses implies a small-diameter propeller and a small mass flow rate of fluid through the propeller. The thrust produced is proportional to the product of the mass flow rate and the change in axial velocity of the fluid passing through the propeller. Therefore, producing a given value of thrust with a small mass flow rate requires large changes in axial velocity and an excessively high slipstream velocity. A discharge jet with a high velocity results in low propulsive efficiency due to the large amount of kinetic energy that is dumped overboard in the jet. The high value of advance coefficient desired to reduce frictional losses requires the transfer of a large component of tangential velocity (swirl) to the fluid. For a small-diameter propeller with a high advance coefficient, large kinetic energy losses are associated with both the axial and tangential components of slipstream velocity which decrease the efficiency of the propulsor.

It is evident that efforts to reduce frictional losses and kinetic energy losses in the slipstream dictate opposing design features. The highest efficiency can be achieved only by a proper balance between them. A more detailed description of the energy losses associated with a conventional propeller and propulsors with a nonswirling slipstream is provided in Appendix I.

## USCG Hulls Considered in the Preliminary Design Studies

It was recommended that two separate USCG boats be considered in the preliminary design analysis. These two boats were a 41 foot utility boat (41' UTB) and an 82 foot patrol boat (82' WPB).

It was the opinion of the USCG that the powering and resistance data of the 41' UTB was more reliable than that of the 82' WPB. This was based on the results of a series of well controlled tests on the 41' UTB whereas the data on the 82' WPB was thought to have more scatter in it.

2

In addition to the powering and resistance data, a number of drawings were furnished which provided details of the shafting and existing propellers on each of the boats. Tables I and II list the powering and resistance data forwarded by the USCG for the design study.

## Preliminary Design Investigation

The provided powering and resistance data in conjunction with the geometrical data of the two boats were used as input to the preliminary design analysis outlined in [1,2] for the standard propeller, reaction fin, and ducted propulsor design studies. The results of these studies provide efficiency, ship speed and propeller diameter as a function of horsepower or shaft speed.

The results are summarized for the 41' UTB in Figures (1-5). Figure (1) represents a typical plot of efficiency versus propeller or rotor diameter for a given horsepower and shaft speed. It is apparent from this plot that the peak efficiency of the reaction fin unit is realized at a smaller propeller diameter than that of the standard propeller. It is also indicated that the reaction fin unit operates with a higher efficiency than that of the propeller.

Shown in Figure (2) is a plot of the ratio of the efficiency of the reaction fin unit and the ducted preswirl to that of the propeller over a range of horsepower. The results indicate that a nominal increase of about 10 percent can be achieved by using a reaction fin type propulsor versus the standard propeller. The ducted preswirl indicates a gain of about five percent in mid-range of horsepower and no gain at the higher power levels.

Figure (3) presents the predicted speeds of the three propulsor types over a range of horsepower. Also plotted are the results of trial data and the comparisons between actual and predicted speeds for the standard propeller are quite good.

3

Table I

Powering and Resistance Data for the 41' Utility Boat

| Shaft RPM | Speed kts | Total Resistance (lbs) | Hp/Shaft | Advance Ratio | $C_D$ Drag Coeff. per Prop | $C_P$ Power Coeff. per Prop | Propulsive Coeff. $\eta\eta$ |
|---|---|---|---|---|---|---|---|
| 800 | 11.65 | 3393 | 115 | .682 | 1.199 | 2.270 | .53 |
| 900 | 14.0 | 4107 | 152 | .728 | 1.005 | 1.729 | .58 |
| 1000 | 16.75 | 4491 | 194 | .784 | .768 | 1.289 | .60 |
| 1100 | 20.0 | 4735 | 230 | .851 | .568 | .897 | .63 |
| 1200 | 22.8 | 5168 | 274 | .889 | .477 | .722 | .66 |
| 1300 | 25.3 | 5829 | 339 | .911 | .437 | .653 | .67 |

$A_{ref} = \frac{\pi}{4} D^2_{ref} = 3.68$

$D_{ref} = 26" = 2.1667$ ft (propeller diameter)

$J \quad = V_\infty/nD$

$C_D \quad = R/1/2\rho V_\omega^2 A_{ref}$

$C_P \quad = Power/1/2\rho V_\infty^3 A_{ref}$

$R \quad = $ Resistance

4

Table II

Powering and Resistance Data for the 82' WPB

| Shaft RPM | Speed (kts) | Total Resistance (lbs) | Hp/Shaft | Advance Ratio | $C_D$ Drag Coeff. per prop | $C_P$ Power Coeff. per prop | Propulsive Coeff. $n_D$ |
|---|---|---|---|---|---|---|---|
| 129 | 4 | 400 | 3.2 | 0.897 | 0.458 | 0.601 | 0.761 |
| 277 | 8 | 2,000 | 36.9 | 0.836 | 0.559 | 0.866 | 0.645 |
| 443 | 12 | 6,000 | 169.8 | 0.784 | 0.764 | 1.18 | 0.647 |
| 618 | 16 | 12,900 | 494.7 | 0.749 | 0.920 | 1.45 | 0.634 |
| 732 | 20 | 16,000 | 757.6 | 0.791 | 0.733 | 1.14 | 0.643 |
| 837 | 24 | 18,300 | 1040.4 | 0.830 | 0.582 | 0.905 | 0.643 |

$D_{ref}$ = 3.5' (propeller diameter)

$A_{ref} = \frac{\pi}{4} D^2_{ref}$ = 9.621'

5

Figure i. Overall Efficiency as a Function of Propeller Diameter (41' UTB)

6
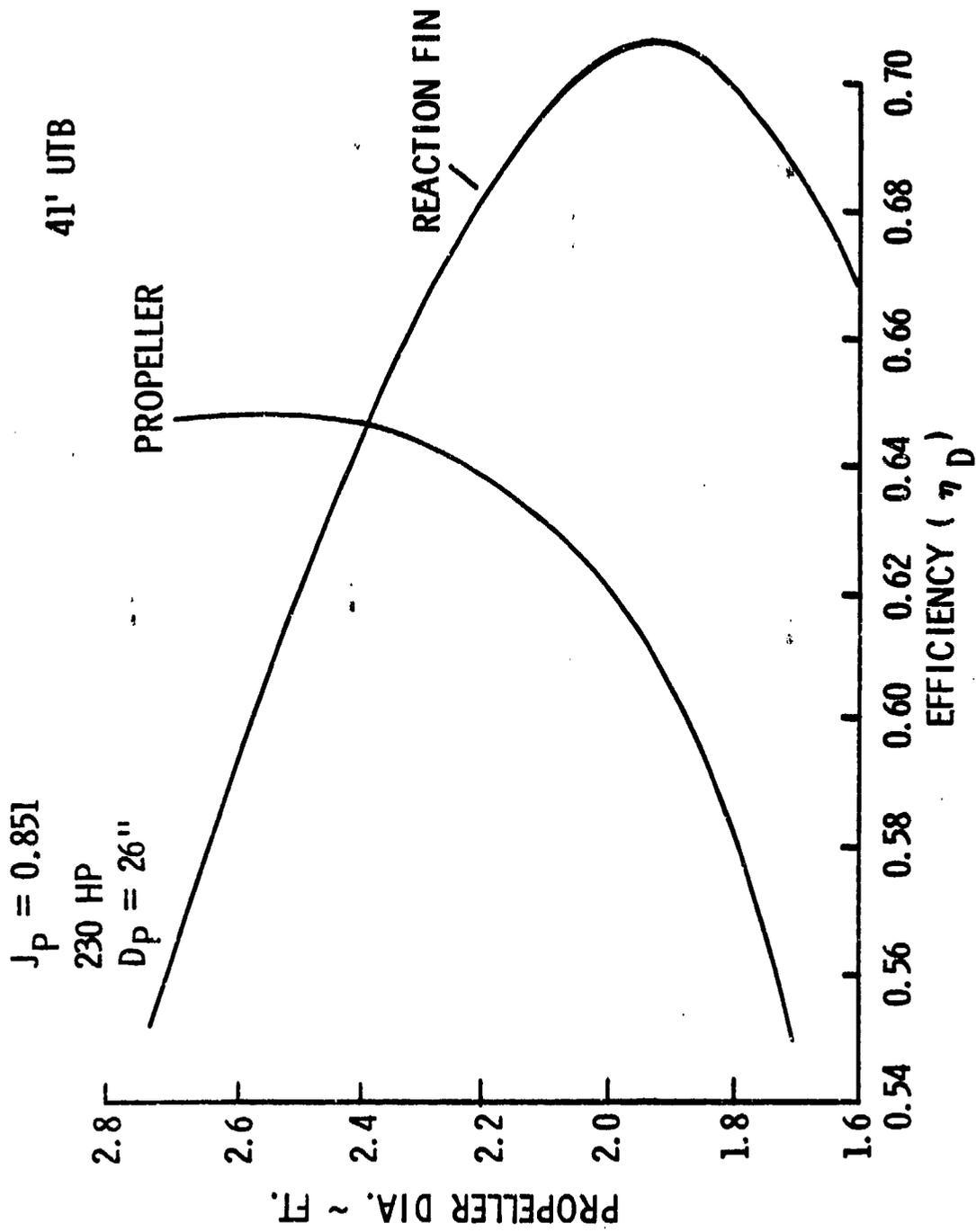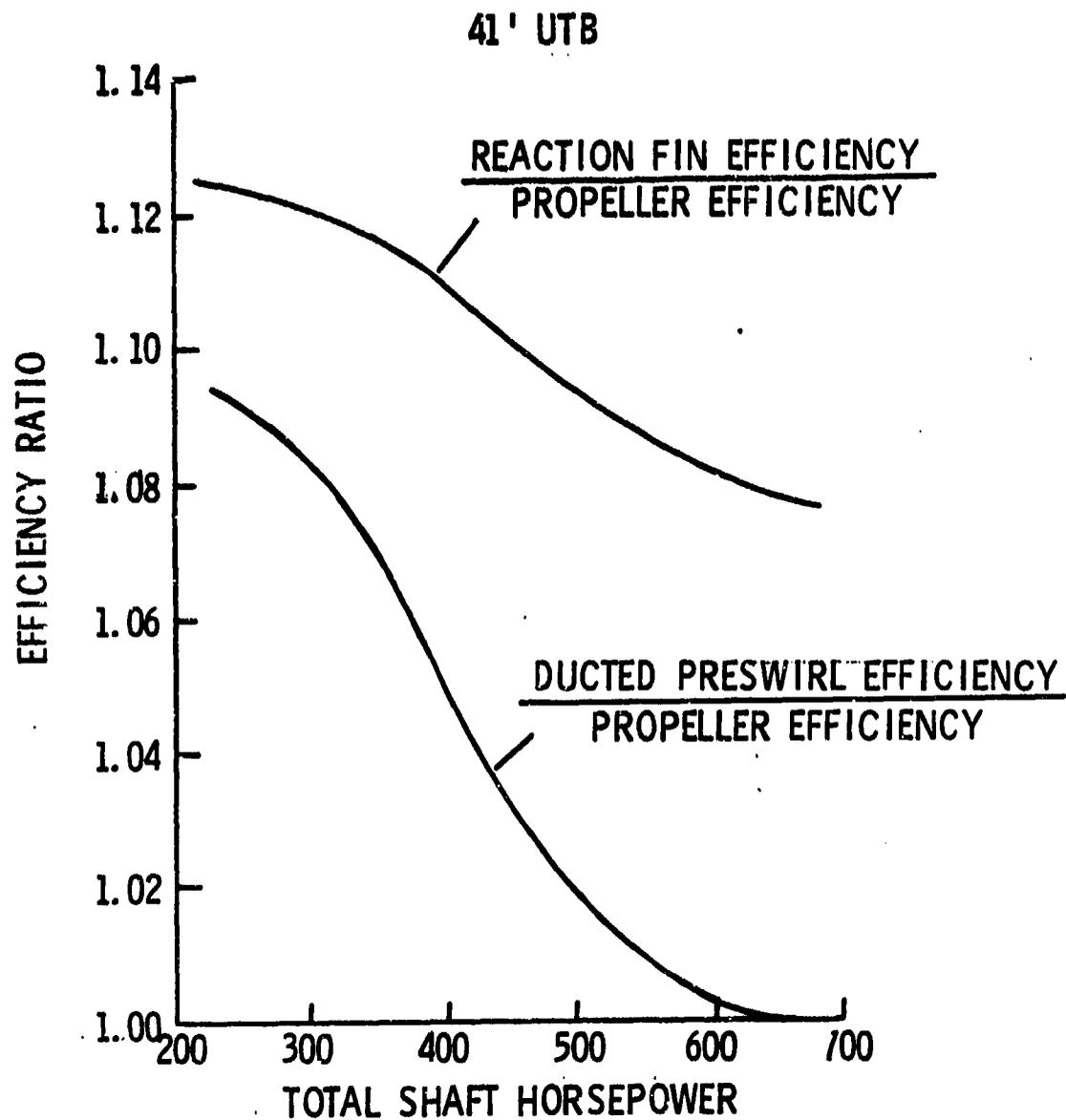
# 41' UTB



Figure 2. Ratio of the Reaction Fin and Ducted Propulsor
Efficiency to That of the Propeller (41' UTB)
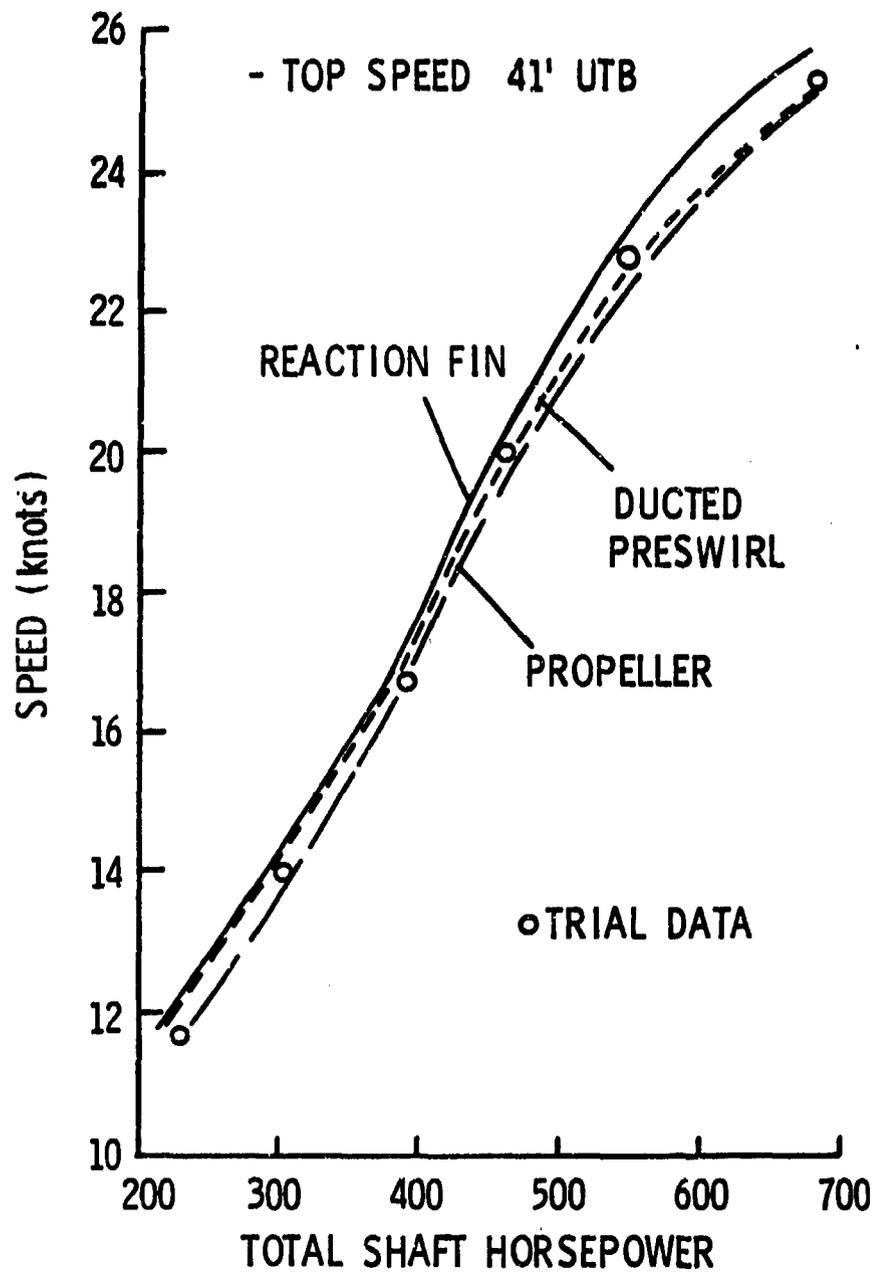
Figure 3. Predicted Ship Speed as Function of Shaft
Power (41' UTB)
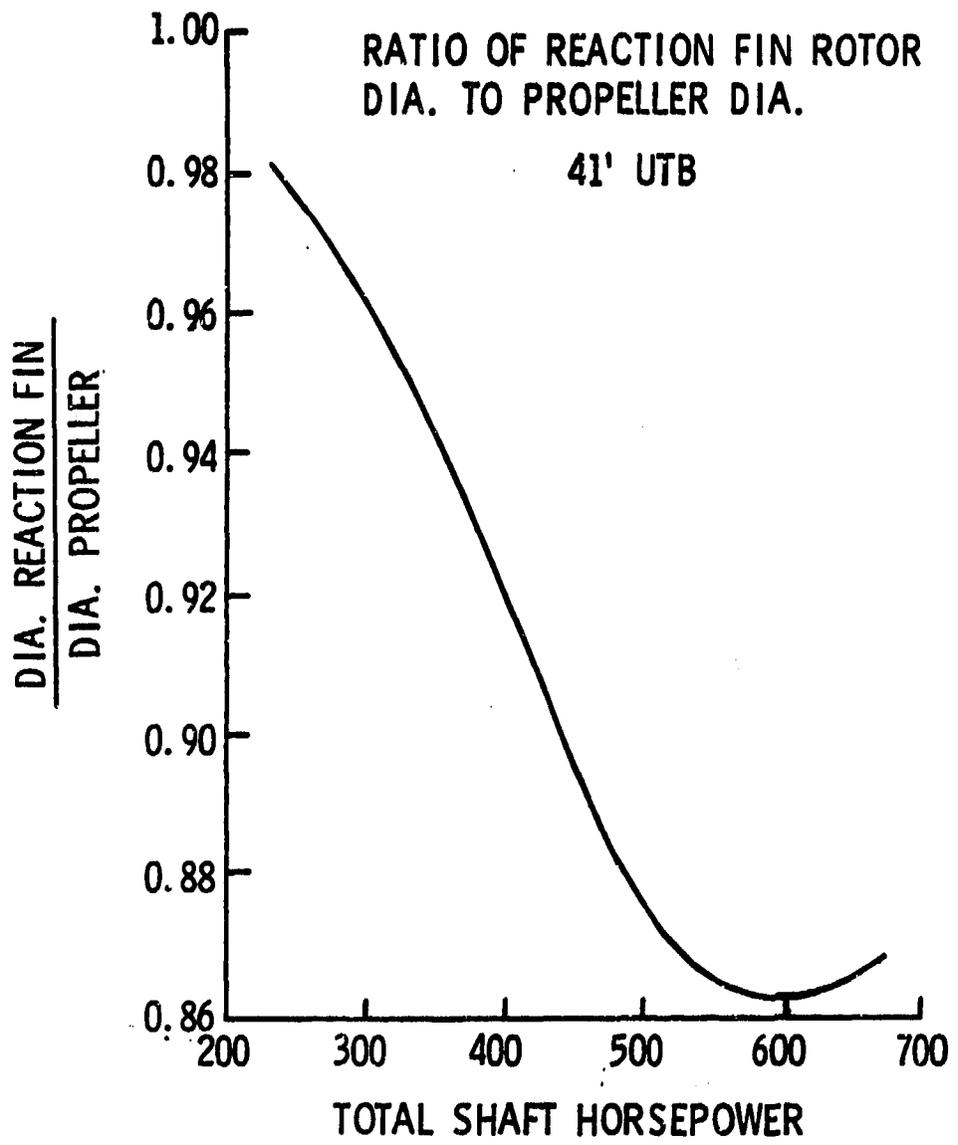
Figure 4. Ratio of Reaction Fin Rotor Diameter to Propeller Diameter (41' UTB) for Peak Efficiency
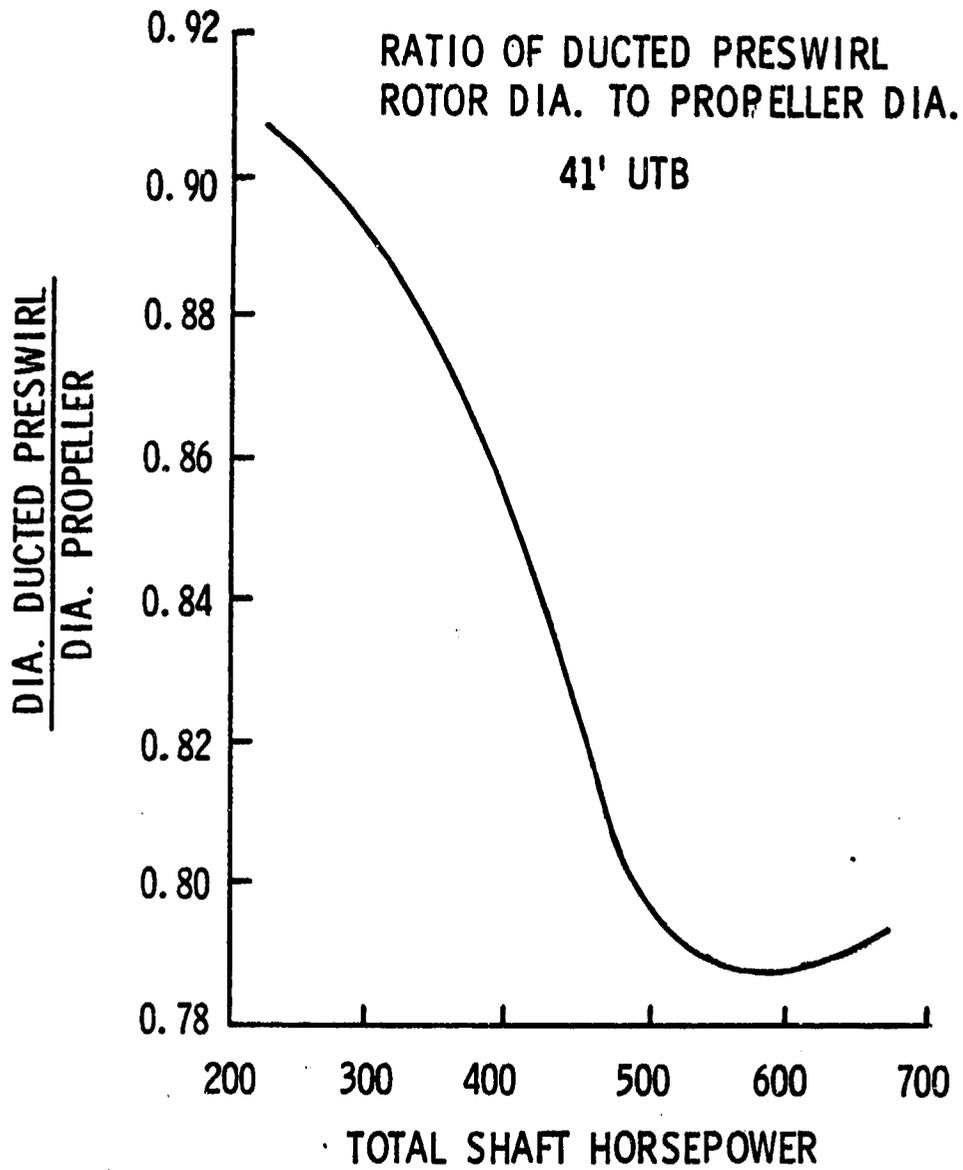
Figure 5. Ratio of Ducted Preswirl Rotor Diameter to
Propeller Diameter (41' UTB) for Peak Efficiency

10
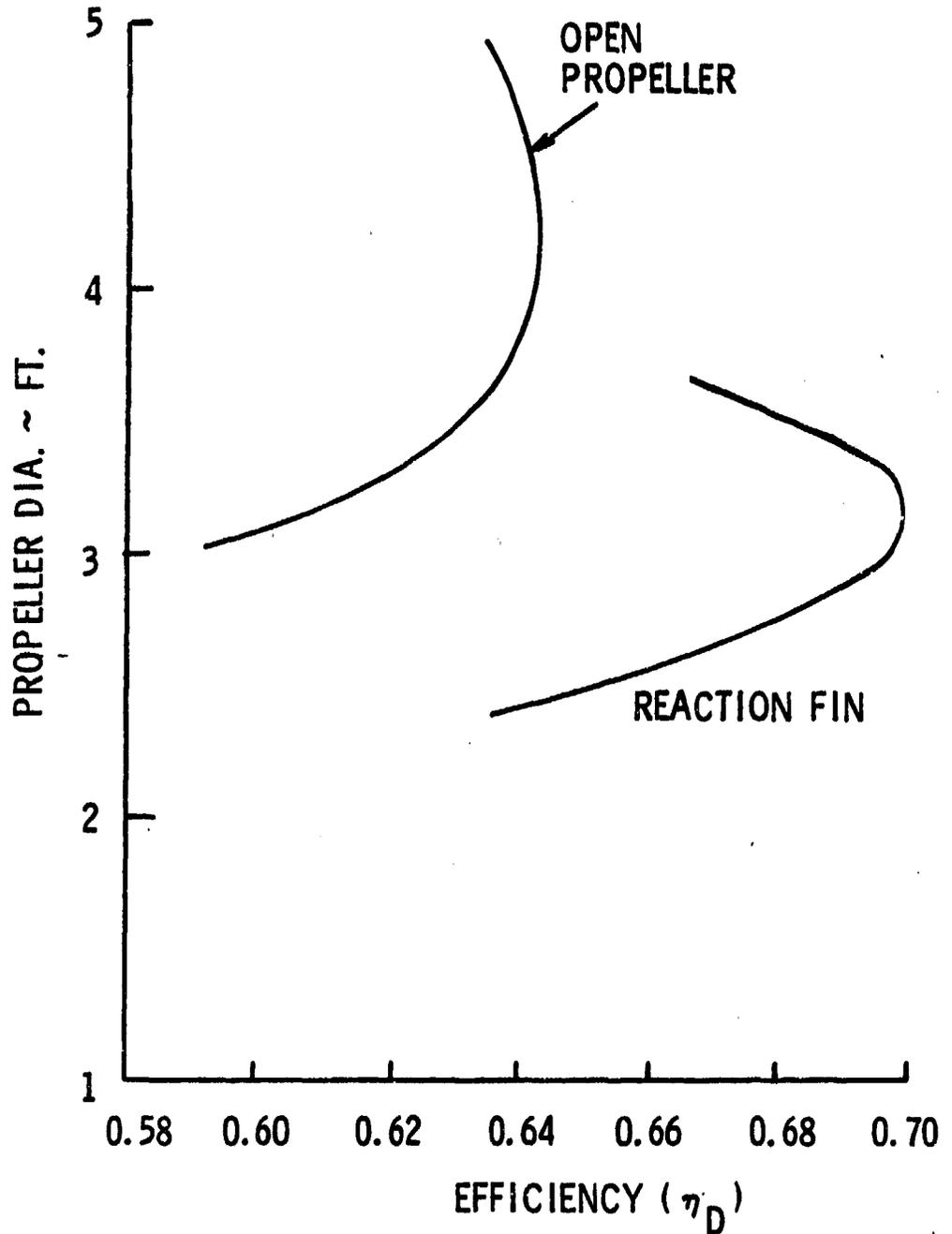
Figure 6. Overall Efficiency as a Function of Propeller Diameter (82' WTB)

## 82 FT. WPB
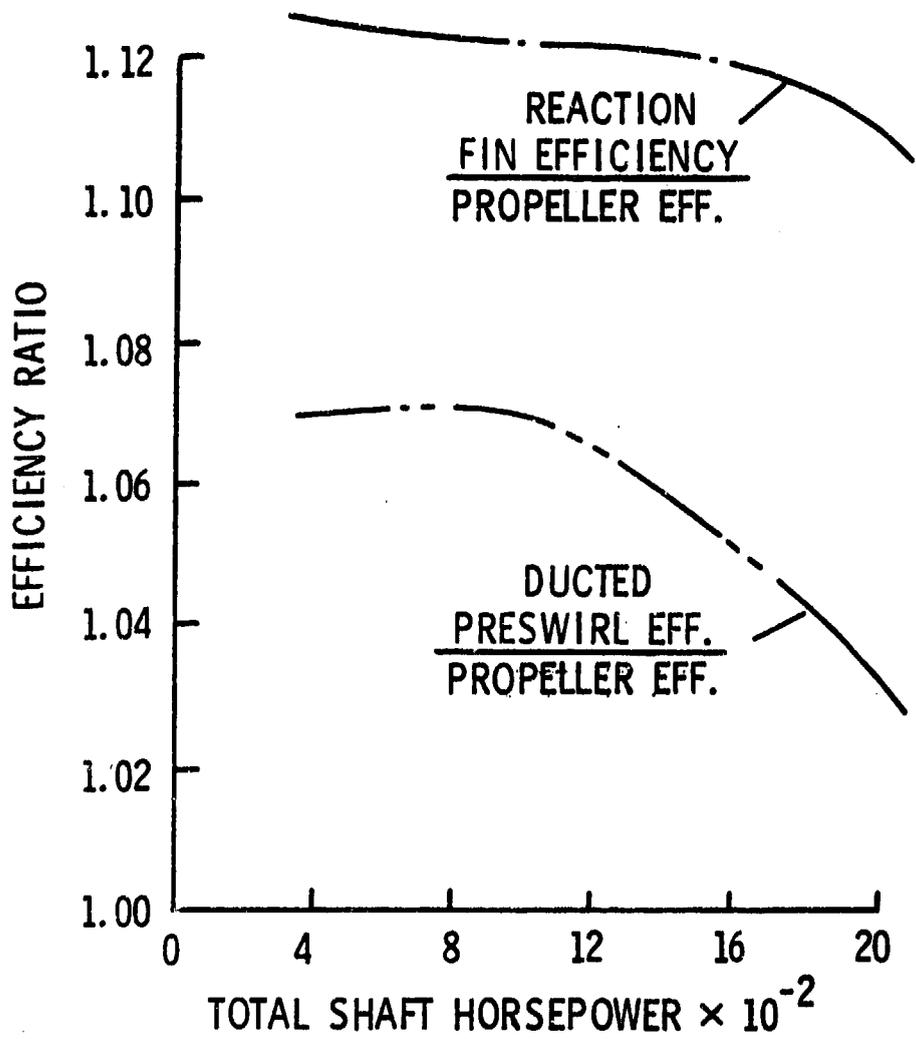


Figure 7. Ratio of the Reaction Fin and Ducted Propulsor Efficiency to that of the Propeller (82' WTB)
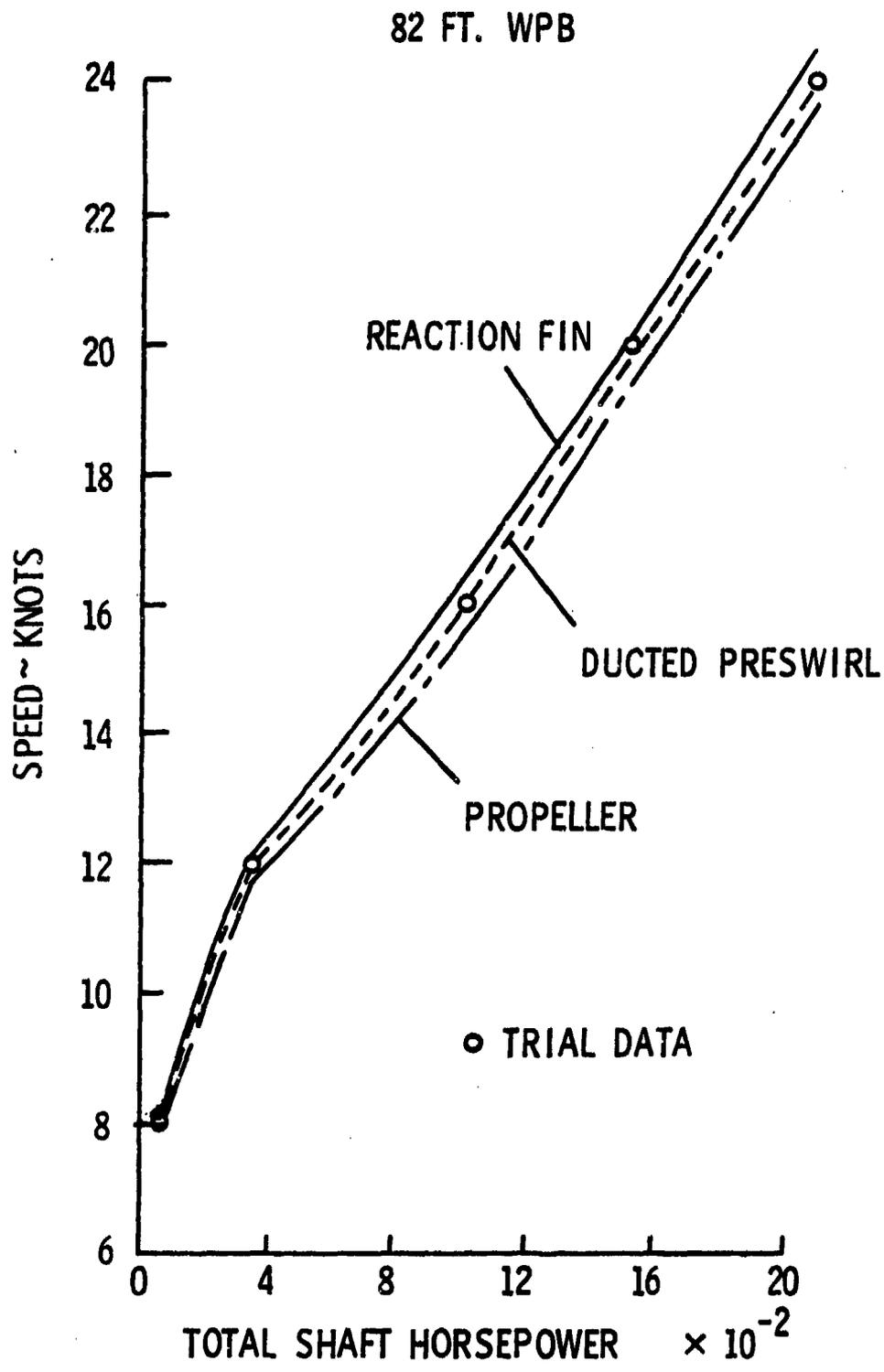
Figure 8. Predicted Ship Speed as a Function of Shaft Power (82' WTB)
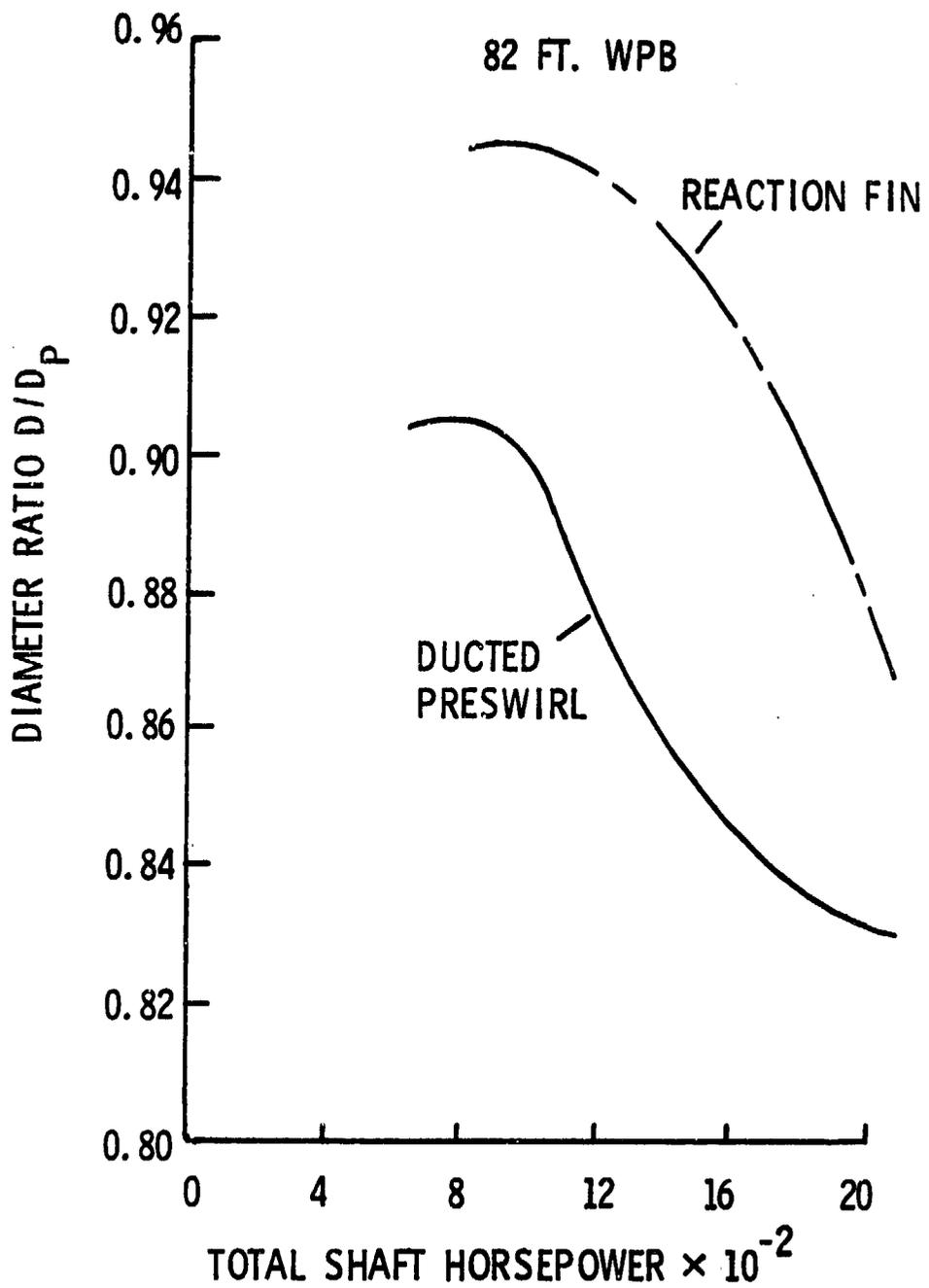
Figure 9. Ratio of Reaction Fin and Ducted Preswirl Rotor
Diameter to Propeller Diameter (82' WPB) for Peak
Efficiency

14

BEARING
SUPPORT
STRUT

COUNTERSWIRL VANE ASSY. MOUNTED
ON SLEEVE WHICH FITS OVER BEARING
HOUSING OF 41' UTB

10"

12"

15
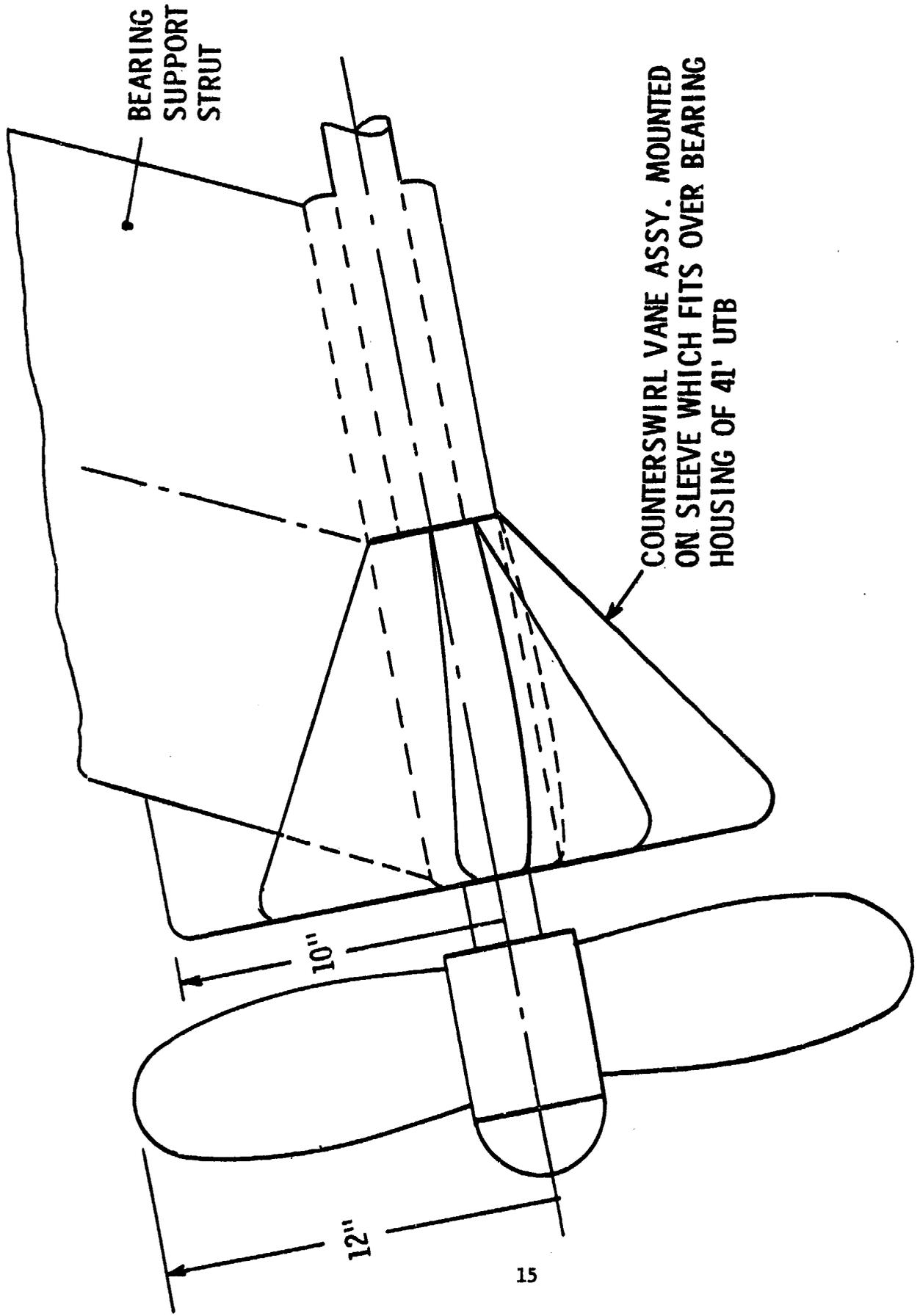
Figure 10.  Schematic of Reaction Fin Arrangement for 41' UTB

As previously discussed the reaction fin and ducted preswirl operate at their peak efficiency when employing a rotor of smaller diameter than that of the standard propeller. This ratio of rotor diameter to standard propeller is shown in Figure (4) and (5) for the reaction fin and ducted preswirl units.

For the 82' WPB, a similar series of curves comparing the efficiencies, ship speeds and propeller diameters are shown in Figures (6-9). In this case the agreement between predicted ship speeds and that obtained from trials for the standard propeller does not agree as closely as for the 41' UTB. This could be attributed to the previously mentioned scatter that was suspected with the 82' WPB trial data.

The results of the preliminary design studies were discussed with the USCG and the following approach was decided upon. The predicted efficiency gains of about 10 percent when employing a reaction fin type unit on the 41' UTB appeared promising. The availability and relative ease of dry docking the 41' UTB for modifications to incorporate a reaction fin type propulsor resulted in selecting this boat for detailed design studies.

A schematic of the proposed reaction fin arrangement for the 41' UTB is shown in Figure (10). The counterswirl vanes are located on the existing bearing housing of the 41' UTB. They shall be shaped to minimize their fouling with debri in the water.

Detailed Design of Reaction Fin Propulsor

The approach used in the design of the reaction fin propulsor consists of obtaining a flow field solution using the "Streamline Curvature Method" described in [3]. This flow field analysis solves the equations of motion to provide the proper spanwise circulation distribution or tangential swirl for both the counterswirl vanes and the propeller. Once the proper circulation on the downstream vanes has been prescribed the propulsor will provide the proper shaft torque and generate the required propelling thrust at a specified shaft speed.

A plot of the streamlines obtained through a typical reaction fin type propulsor using the described flow field solution is shown in Figure (11). The lines which are close to vertical represent computational stations for the flow field solution. The axial and tangential components of velocity downstream of the counterswirl vanes and downstream of the rotor are shown in Figures (12) and (13). The counterswirl vanes place swirl in the flow that is counter to rotor rotation over the inner 80 percent of the rotor span. The action of the rotor removes this swirl and as evidenced by Figure (13) the swirl in the slipstream far downstream of the rotor is essentially zero.

Also plotted on Figure (13) in dashed lines is the swirl distribution and axial velocity that would exist in the slipstream if no counterswirl vanes were employed. It is the elimination of this swirl that results in the efficiency gain that is predicted for the reaction fin propulsor.

The design parameters of the rotor of the reaction fin propulsor is provided by Table III and detailed in ARL/PSU Drawing SKR 89433. The rotor was designed to fit on the existing shafting of the 41' UTB. The maximum stress was 12,000 psi and occurs in the root section of the propeller at a power level corresponding to 23 kts. This stress level assumed no fillets in the root sections and is therefore on the conservative side.

The cavitation performance of the redesigned propulsor was evaluated in several ways. The first consisted of a criteria by "Barnaby" listed in [4] which limits the ratio of thrust to projected propeller area to a value not to exceed 13 psi. This ratio when evaluated for the reaction fin rotors at 20 kts was found to be 9.4 psi, thereby satisfying this criteria.

A second method of evaluating propeller performance is that of "Burrill" as described in [4]. In this method a limiting value of cavitation number is plotted against a ratio of thrust per unit of projected blade area. For the reaction fin propeller, the ratio of thrust to projected blade area divided by the dynamic head relative to the blade at 0.7 R was computed to be 0.182 at 20 kts. The cavitation number consists of

17

STREAMLINES

COUNTERSWIRL
VANES

ROTOR
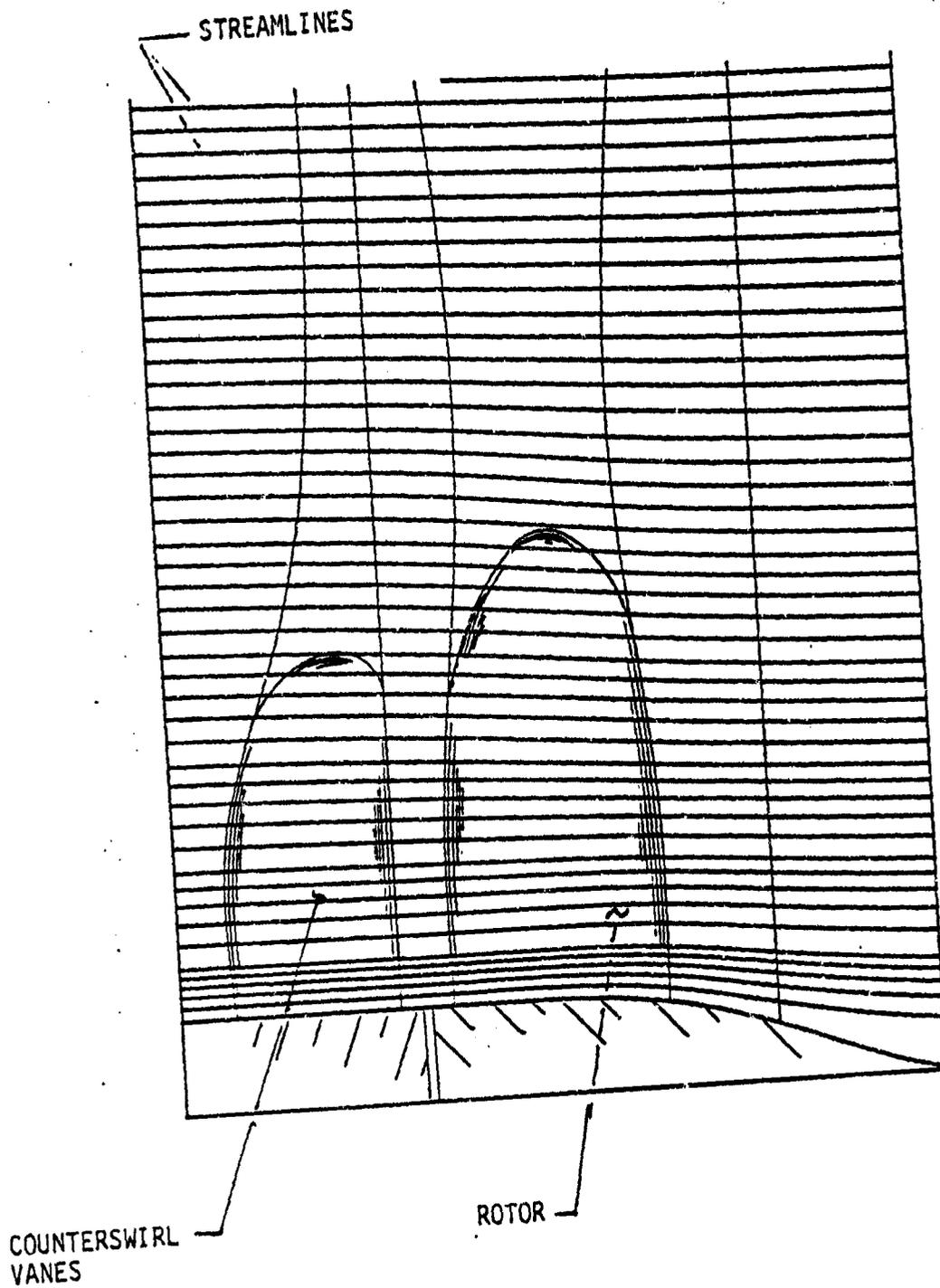
Figure 11. Streamlines Through Reaction Fin Propulsor

18
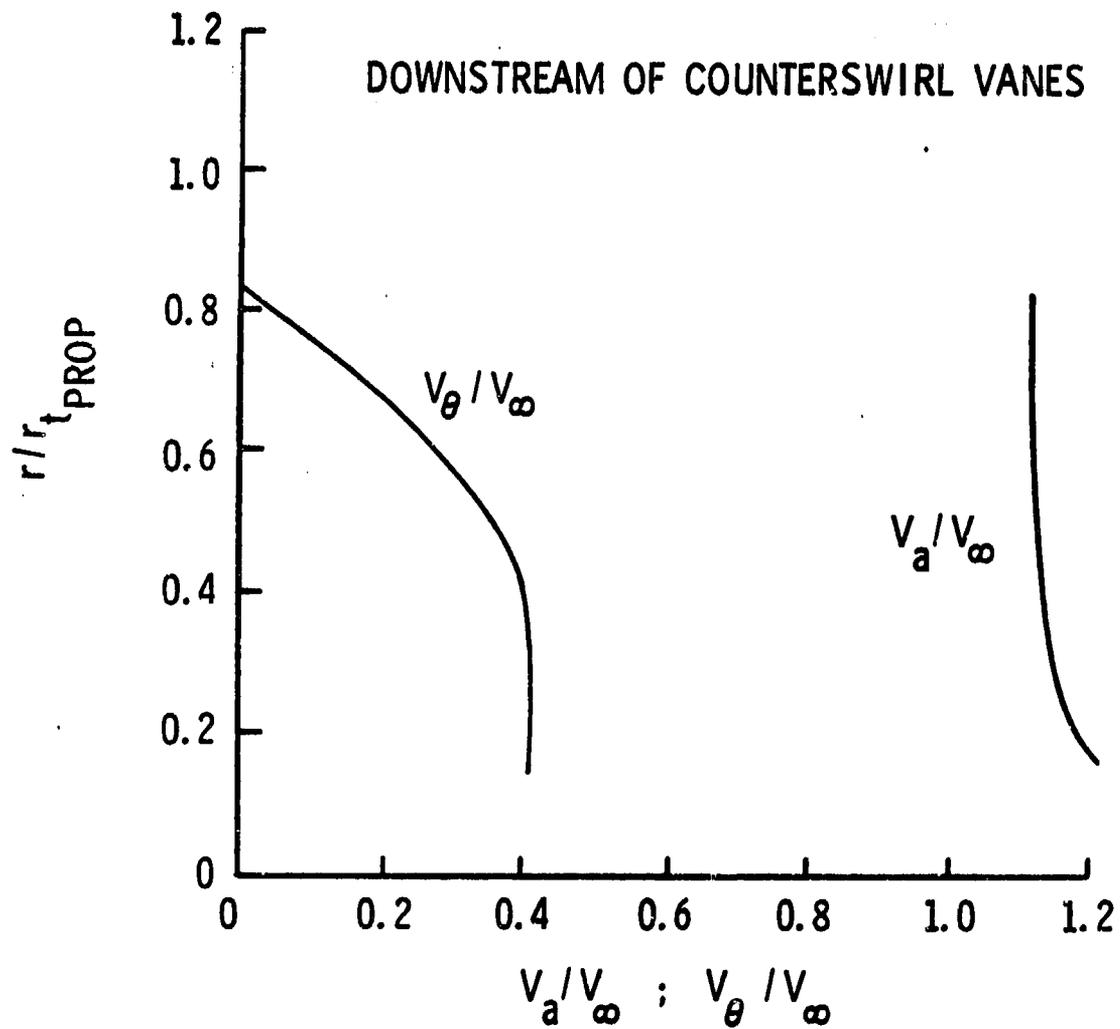
Figure 12.   Axial and Tangential Velocity Distribution
Downstream of Counterswirl Vanes

FAR DOWNSTREAM OF PROPELLER

--- WITHOUT COUNTERSWIRL
——— WITH COUNTERSWIRL

$V_a/V_\infty$

$V_\theta/V_\infty$

$V_a/V_\infty$ ; $V_\theta/V_\infty$

$r/r_{t_{PROP}}$
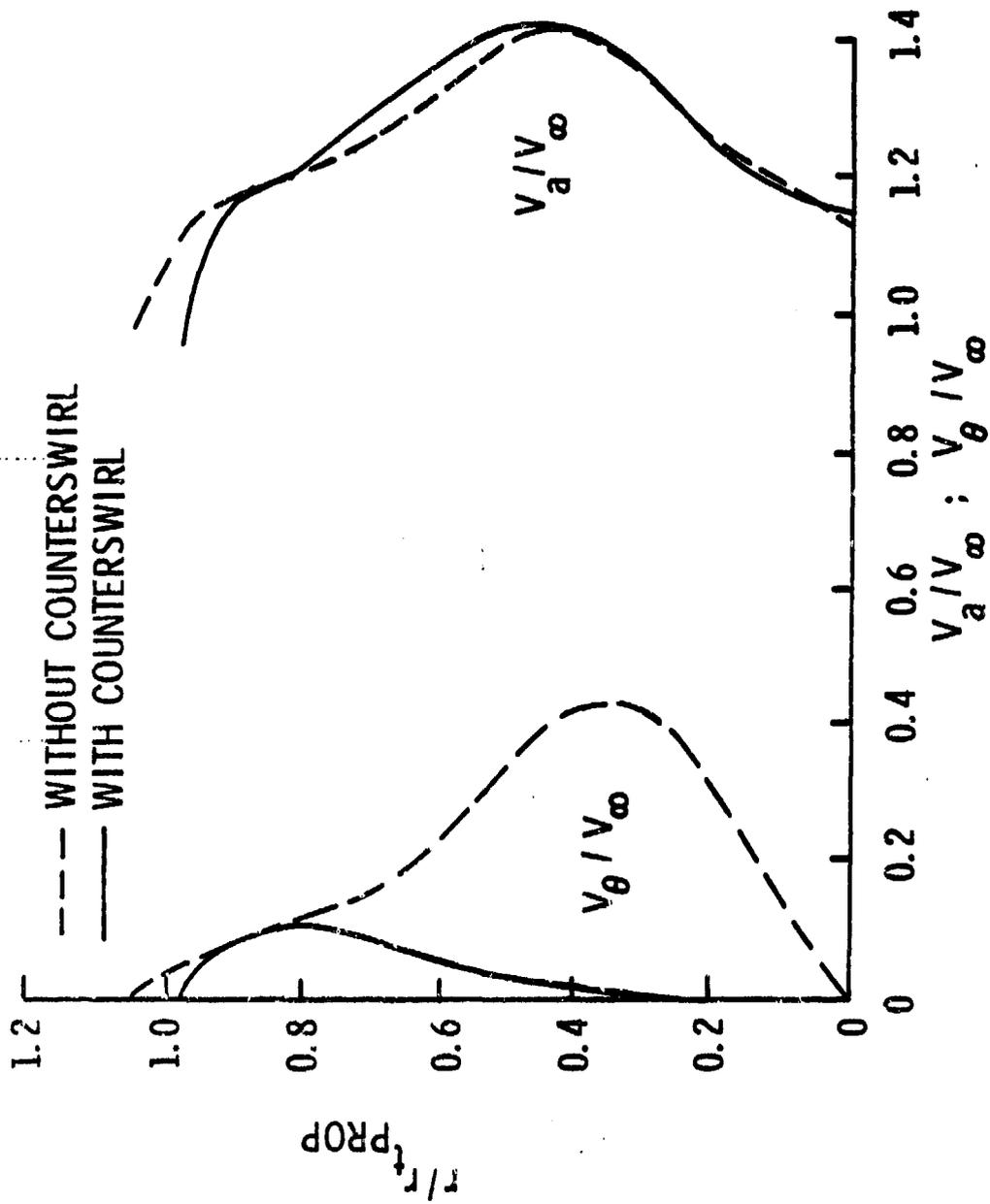
Figure 13. Axial and Tangential Velocity Distribution Downstream of Rotor

Table III

USCG REACTION FIN PROPULSOR
RIGHT HANDED PROP

Diameter = 24.0 inches

Cylindrical Sections

N = 5 Blades
NACA 65 Mean Line
NACA 65 Basic Thickness

| r/R | Chord/Dia. | Thickness/Dia. | Camber/Dia. | Pitch Angle | Skew* | Rake | $G_s = \frac{\Gamma}{2\pi r_T V_\infty}$ |
|---|---|---|---|---|---|---|---|
| 0.2 | 0.21354 | 0.04037 | 0.00391 | 53.30000 | -1.43750 | 0.0 | 0.0168 |
| 0.3 | C.27344 | 0.03646 | 0.00521 | 44.20000 | -1.50000 | 0.0 | 0.0256 |
| 0.4 | 0.32682 | 0.03125 | 0.00521 | 38.00000 | -1.60930 | 0.0 | 0.0320 |
| 0.5 | 0.35157 | 0.02733 | 0.00846 | 33.60000 | -1.46880 | 0.0 | 0.0356 |
| 0.6 | 0.35808 | 0.02208 | 0.00717 | 29.90000 | -1.23440 | 0.0 | 0.0354 |
| 0.7 | 0.34505 | 0.01825 | 0.00625 | 26.60000 | -0.92185 | 0.0 | 0.0300 |
| 0.8 | 0.30208 | 0.01300 | 0.00521 | 23.60000 | -0.46875 | 0.0 | 0.0236 |
| 0.9 | 0.21354 | 0.01042 | 0.00260 | 21.00000 | +0.12500 | 0.0 | 0.0132 |
| 0.95 | 0.14844 | 0.00781 | 0.00130 | 19.80000 | +0.40620 | 0.0 | 0.0068 |

*Skew is in aft direction.

a ratio of absolute head above vapor pressure at the propeller divided by
the dynamic head based on the velocity relative to the blade at 0.7 R. The
cavitation number for the reaction fin propeller was 0.298 at 20 kts. The
cavitation resistance of the proposed reaction fin propeller, based on the
"Burrill" criteria, indicates it would have limited cavitation at 20 kts but
not of sufficient magnitude to result in thrust decrease or breakdown.

Table IV lists comparative characteristics of the existing propeller
and the proposed reaction fin rotor.

The design of the stationary reaction fins was strongly influenced by
practical engineering considerations. First the frequent operation of the
41' UTB in waters filled with debri required a geometry that would resist
fouling. This resulted in a fin with a large degree of leading edge rake as
depicted in Figure (10).

The angle of shaft inclination with respect to the bottom of the boat
hull is 13 degrees. This results in the propeller or rotor operating in an
oblique flow. (i.e. The inflow to the propeller is not normal to the plane
of the propeller.) The oblique flow induces a component of velocity in the
plane of the propeller as depicted schematically in Figure (14). The
consequence of this induced velocity is such that as the propeller rotates
through one revolution it alternately sees a reduction in angle of attack or
incidence in the left two quadrants, from 180 to 360 degrees. Conversely,
it operates at an increase incidence from 0 to 180 degrees.

It is emphasized that in the quadrant from 0 to 180 degrees that
counterswirl is induced into the flow due to the obliqueness of the inflow
relative to the plane of the propeller. The counterswirl is of a magnitude
that no counterswirl vanes are required in this region. However, in the
quadrant from 180° to 360 degrees counterswirl vanes are required. These
vanes must remove the velocity induced by the oblique flow and impose an
additional increment of counterswirl that the action of the propeller will
remove. This arrangement will provide a slipstream with essentially zero

Table IV

Propeller Characteristics of Existing 41' UTB Propeller and Reaction Fin Propeller

| | Dia | Blade Number | Expanded Area Ratio | Projected Area Ratio | Weight | HP @ 20 Kts |
|---|---|---|---|---|---|---|
| Existing Propeller | 26" | 4 | 0.727 | ---- | 55# | 460 |
| Reaction Fin Propeller | 24" | 5 | 0.734 | 0.590 | 63# | 422 |

Pitch of Existing Propeller is Constant at 28.0"

Pitch of Proposed Reaction Fin Rotor Varies Over Span as Indicated on Drawing #SKR 89433

STARBOARD SIDE

SHIP HULL

SHAFT SUPPORT STRUT

OBLIQUE INFLOW TO PROPELLER

13⁰

OUTBOARD VIEW

270⁰

90⁰

0⁰

180⁰

DIRECTION OF PROP. ROTATION
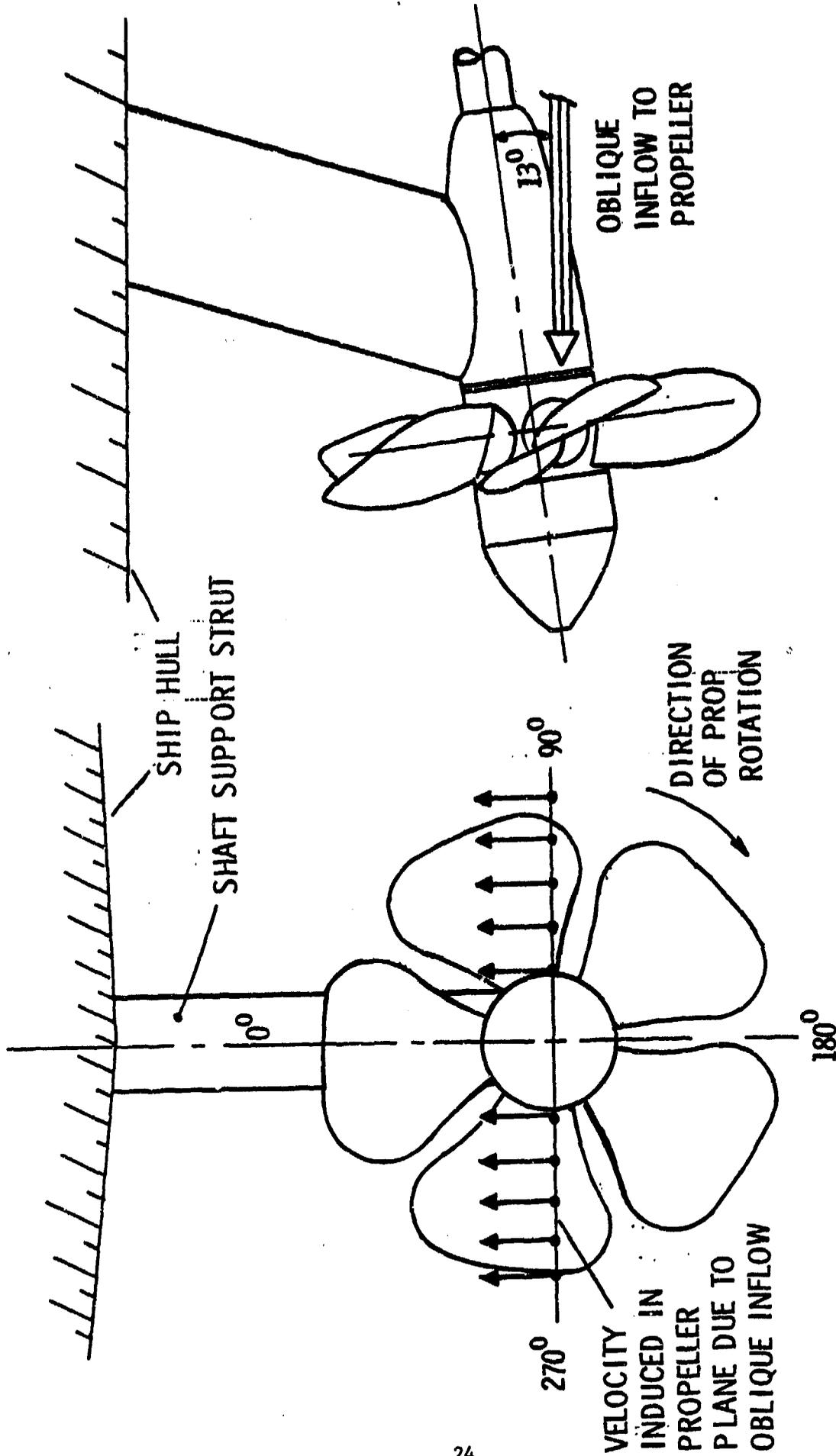
VELOCITY INDUCED IN PROPELLER PLANE DUE TO OBLIQUE INFLOW

VIEW LOOKING FORWARD

Figure 14. Flow Induced in Plane of Propeller Due to Oblique Flow (Starboard Side)

24

swirl. In the design of the preswirl vanes the effects of vane loading and vane geometry modify the shape and magnitude of the distortion prior to its entry into the propeller.

A schematic of the proposed reaction fin propulsor for the 41' UTB is shown in Figure (15). The stationary vane system consists of five counterswirl vanes located upstream of a five bladed rotor. One of the counterswirl vanes will be fabricated by adding a fairing to the aft of bearing support strut. The two counterswirl vanes located on the side of the bearing housing shall be of the same geometry. The two counterswirl vanes located near the bottom of the bearing housing shall differ in geometry from those on the side but be identical to each other. On this basis it is envisioned that sand cast counterswirl vanes of only two separate geometries will be required for each shaft. Thus for the twin shafted 41' UTB, the number of patterns required for casting the counterswirl vanes would be four, which would provide two separate blade geometries for each shaft. The design parameters of the two reaction vanes located in the left hand quadrant of Figure (15) are listed in Table V. The design parameters of the two reaction vanes located in the bottom quandrant of Figure (15) are listed in Table VI. ARL/PSU drawings detail the geometry of the reaction fins. The maximum stress in the stationary vanes was 2,500 psi at 20 kts.

A concern with respect to unsteady shaft forces arises since the design consists of five upstream vanes and a five bladed rotor. However the wake pattern flowing into the propeller really has a sixth distortion originating from the oblique flow in the quadrant from 0 to 180°. The counterswirl vanes are not positioned at equal circumferential distances apart. Therefore it is estimated a sufficient mismatch of the harmonic content of the inflow to the propeller will be obtained with respect to the five bladed propeller.

The level of vibration which the existing standard propeller arrangement produces in rotating through the large single cycle distortion created by the oblique flow is estimated to be significantly reduced with

25

COUNTERSWIRL VANE ASSEMBLY

SHAFT SUPPORT STRUT

SHIP HULL

PROPELLER

COUNTERSWIRL VANES

DIRECTION OF PROPELLER ROTATION
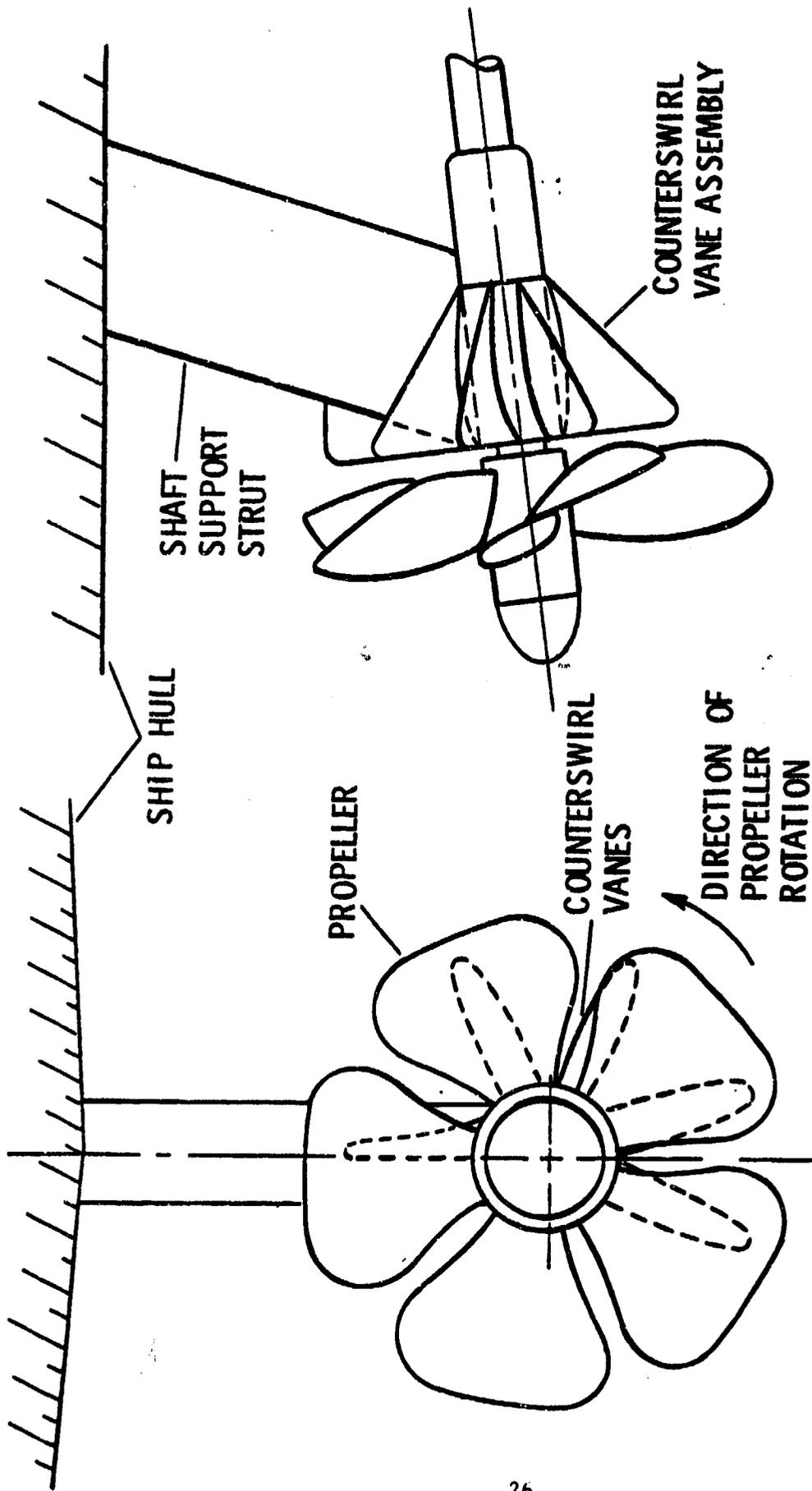
VIEW LOOKING FORWARD

Figure 15. Schematic of Proposed Reaction Fin Propulsor for (41' UTB)

26

Table V

USCG REACTION FIN BLADES 1 & 2
RIGHT HAND ASSEMBLY

Diameter = 20.0 inches

Rectangular Sections

N = 2 Blades
NACA 65 Mean Line
NACA 65 Basic Thickness

| r/R | Chord/Dia. | Thickness/Dia. | Camber/Dia. | Pitch Angle | X Shift* | Y Shift** | $G_s = \dfrac{\Gamma}{2\pi r T V_\infty}$ |
|---|---|---|---|---|---|---|---|
| 0.25 | 0.51500 | 0.03925 | 0.03563 | 88.00000 | -1.44338 | +0.43012 | -0.060 |
| 0.49 | 0.37574 | 0.03282 | 0.02415 | 88.67606 | -2.82902 | -0.25807 | -0.110 |
| 0.725 | 0.24149 | 0.02561 | 0.01665 | 89.33803 | -4.18579 | -0.93192 | -0.123 |
| 0.96 | 0.10631 | 0.01550 | 0.00750 | 90.00000 | -5.54256 | -1.16058 | -0.040 |

* X Shift is in forward direction (see Figure 16).

**Y Shift is in port direction looking forward.

27

Table VI

USCG REACTION FIN BLADES 3 & 4
RIGHT HAND ASSEMBLY

Diameter = 20.0 inches

Rectangular Sections

N = 2 Blades
NACA 65 Mean Line
NACA 65 Basic Thickness

| r/R | Chord/Dia. | Thickness/Dia. | Camber/Dia. | Pitch Angle | X Shift* | Y Shift** | $G_s = \dfrac{\Gamma}{2\pi r V_\infty}$ |
|------|-----------|----------------|-------------|-------------|----------|-----------|------|
| 0.25 | 0.51500 | 0.03925 | 0.02165 | 85.00000 | -1.44338 | +0.12466 | -0.045 |
| 0.49 | 0.37674 | 0.03282 | 0.01583 | 85.00000 | -2.82902 | -0.47372 | -0.083 |
| 0.725 | 0.24149 | 0.02561 | 0.01250 | 85.00000 | -4.18579 | -1.05964 | -0.093 |
| 0.96 | 0.10631 | 0.01550 | 0.00625 | 85.00000 | -5.54256 | -1.64556 | -0.030 |

* X Shift is in forward direction (see Figure 16).

**Y Shift is in port direction looking forward.

28
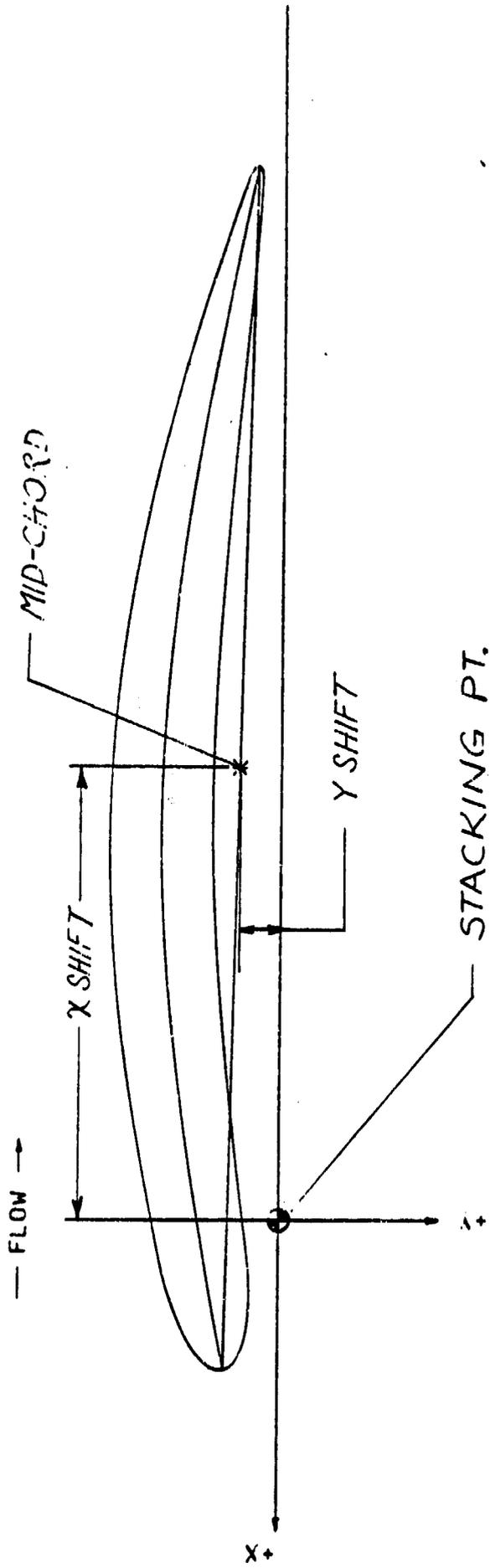
Figure 16. Schematic of Blade Shift Relative to Stacking Point

29

the proposed reaction fin propulsor. This is based on the attenuation of the one cycle distortion that is achieved by using the counterswirl vanes.

## Comparison of Cruising, Towing and Low Speed Operation

A series of water tunnel tests have been performed on an arrangement similar to that shown in Figure (10). Propeller shaft torque and net axial thrust applied to the ship were measured over a wide range of advance ratios. An advance ratio corresponding to zero represents a case where the ship is "dead in the water" and some finite shaft speed exists (i.e. a bollard pull condition). The design advance ratio for the unit shown in Figure (17) was about 1.2. Figure (17) is a plot of net axial force coefficient versus advance ratio. It is apparent, for a given shaft rpm, the reaction fin unit produces equal or slightly greater thrust over the entire range of advance ratios tested. On this basis it is concluded that the towing and low speed operation of the reaction fin propulsor will be equal or better than that of the standard propeller.

## Test and Evaluation Plan

The following is an outline of experimental measurements recommended to obtain comparative performance between the standard propeller and reaction fin unit.

The comparative performance between the standard propeller and the reaction fin propulsor is the objective of the trial evaluation. On this basis it is recommended that all discussed measurements be obtained with the same 41' UTB having the same hull condition and draft. This also implies testing in the same current and wind conditions. Tests and data would be obtained with the standard propeller on the selected boat. The boat would then be drydocked and the reaction fin propulsor installed for similar tests. It is imperative that a sufficient number of tests be repeated to provide a good statistical average.

## OFF-DESIGN PERFORMANCE
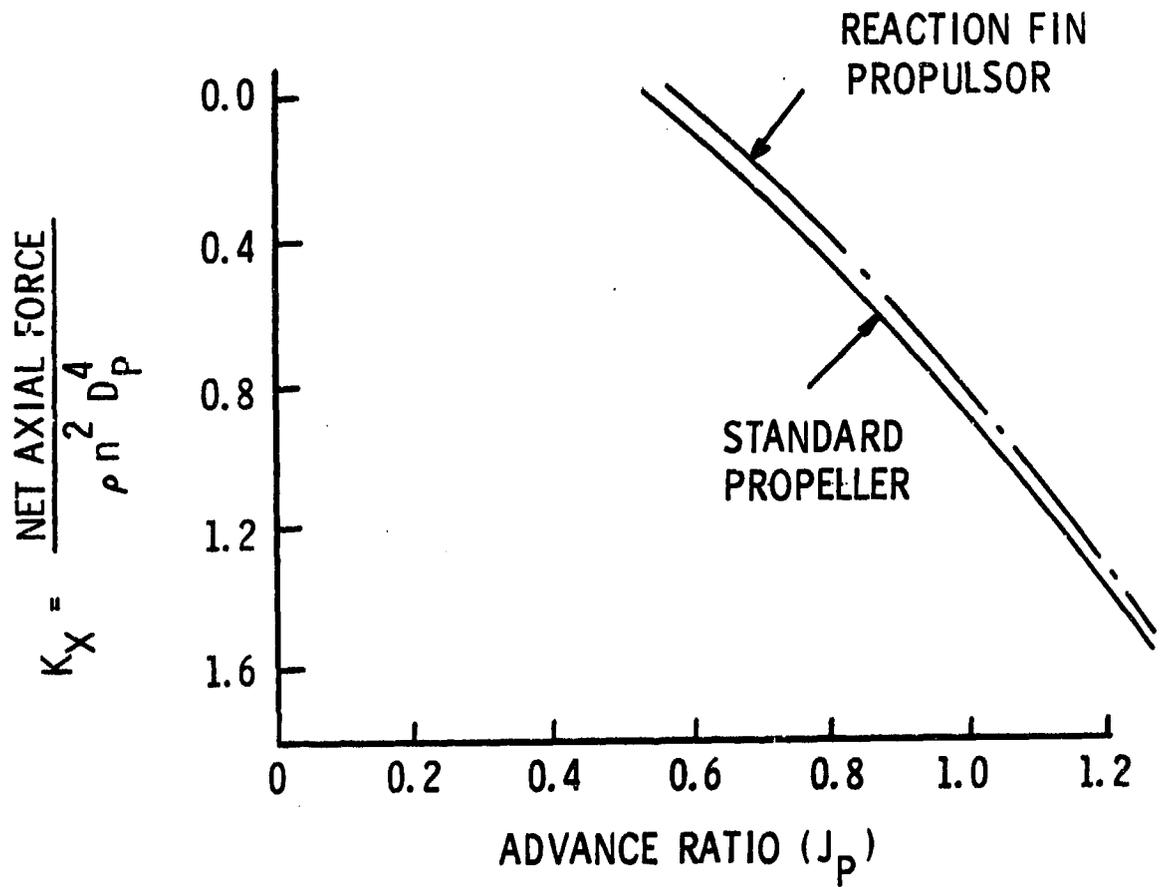


Figure 17. Net Axial Force Imparted to Ship with Standard Propeller and Reaction Fin Propulsor at Off-Design Conditions

It is emphasized that the camber of the stationary counterswirl vanes is such as to provide about 1,200 lbs of lift to the boat at a speed of 20 Kts. This force may change the trim of the boat slightly at high speeds.

The unsteady pressure on the hull near the propeller should be reduced since the variation in flow incidence has been reduced as the propeller rotates through one revolution. To verify the degree of unsteady pressure reduction it is proposed to mount one or more unsteady pressure transducers on the hull near the plane of the propeller. It is also proposed that accelerometers be mounted on the interior of the hull and on the shaft thrust bearing or housing to monitor vibration levels.

Shaft torque and rpm measurements will provide a measurement of shaft power. This combined with ship speed obtained by time lapse between control points will provide relative levels of efficiency.

A separate check on efficiency could be obtained by monitoring fuel usage as a function of shaft rpm and/or ship speed. This would probably be required over a rather extended period of operation to obtain a more accurate value.

An acoustic transducer (i.e. high frequency response) located on the bearing support strut or possibly inside the hull directly above the propeller could provide an indication of cavitation inception as a function of ship speed.

The rotor shaft thrust for the reaction fin propulsor will be higher than that of the standard propeller for a given ship speed. This results from the reduced static pressure in front of the propeller created by the swirl placed in the flow by the counterswirl vanes. The measurement of shaft thrust does not indicate the efficiency of the reaction fin propulsor relative to the standard propeller. It is therefore recommended that shaft thrust measurement be neglected.

32

The fouling characteristics of the two propulsors arrangements should be evaluated if a reasonable test can be proposed.

A bollard pull test where a load cell is installed between a line fastened to a dock, etc. could be monitored as a function of shaft rpm. This would indicate towing characteristics of both units.

The unsteady and acoustic measurements previously discussed should be monitored at a given shaft speed and a fixed or prescribed rate of turning applied to the boat. This would indicate impact of the reaction fin unit on cavitation inception and vibrations during maneuvers.

The presence of the stationary counterswirl vanes may act to reduce buffeting in choppy waters. Accelerometer measurements at a given shaft speed in different sea states are recommended.

The instrumentation and test procedures recommended are relatively straight forward; however, it is envisioned that acoustic measurement of propeller cavitation inception could be masked should cavitation occur at some location other than on the propulsor. The only alternative is visual observation which would require relatively expensive and sophisticated instrumentation.

The proposed measurements and their results could significantly guide in the design and use of the reaction fin propulsor for application on other boats and therefore the test program is of major importance.

Summary

Preliminary design studies were performed considering a standard propeller, a reaction fin propulsor as shown in Figure (10) and a ducted propulsor for application on a 41' UTB and a 82' WPB. A review of these studies and discussions with the USCG program monitor resulted in a decision to proceed with detailed design of a reaction fin propulsor for application on the 41' UTB.

The reaction fin propulsor indicated an efficiency gain of about 10 percent relative to the standard propeller now used.

The diameter of the reaction fin propeller is 24.0" versus 26.0" for the existing standard propeller.

The detailed design of the reaction fin rotor indicated a five-bladed propeller was required whose pitch varied along its span. The existing standard propeller is a four-bladed unit which has a constant pitch with respect to span.

A stationary set of counterswirl vanes were designed and consisted of five vanes. The spacing and location about the axis of rotation of these vanes were not symmetrical as indicated by Figure (15).

The swirling motion imparted to the flow by the stationary counterswirl vanes is intended to reduce the magnitude of the flow distortions that presently exist in the inflow to the standard propeller. This should provide reduced levels of hull vibration and cavitation inception when the reaction fin propulsor is employed on the 41' UTB.

Experimental measurements on propulsor arrangements similar to the proposed reaction fin propulsor indicate that performance during low speed and towing operations should not be degraded when using the reaction fin propulsor.

The presence of the stationary counterswirl fins could act as damping surfaces to attenuate ship accelerations and vibration during operation in choppy waters.

Hydrodynamic specification of the reaction fin propulsor has been provided in sufficient detail to permit its mechanical design for fabrication and application on the 41' UTB.

## Acknowledgement

## References

[1] Gearhart, W. S. and E. P. Bruce, "Thrusting Characteristics of Propulsors," Applied Research Laboratory TM 80-118, May 30, 1980.

[2] Bruce, E. P., W. S. Gearhart, J. R. Ross and A. L. Treaster, "The Design of Pumpjets for Hydrodynamic Propulsion," NASA SP-304, 1974.

[3] McBride, M. W., "The Design and Analysis of Turbomachinery in an Incompressible, Steady Flow Using the Streamline Curvature Method," Applied Research Laboratory TM 79-33, February 13, 1979.

[4] Von Lammeran, W. P. A., Troost, L. and Koning, J. C., Resistance, Propulsion and Steering of Ships, Vol. II, The Technical Publishing Co., H. Stam-Harrlem-Holland, 1948.

## Differences Between the Standard Propeller and Propulsors Employing Counterswirl

The primary difference between the conventional propeller and unducted or ducted propulsors employing counterswirl is that the propeller discharges a slipstream which has swirl in it whereas the others do not.

If the energy losses associated with the slipstream are considered, it can be better appreciated why some propulsor configurations which discharge a slipstream with zero swirl have advantages with regard to both efficiency and cavitation performance.

Figure (18) shows the sources of energy losses in a propeller slipstream:

(a) axial kinetic energy loss, and

(b) reduced pressure due to swirl in the slipstream.

The axial kinetic energy loss results from the axial component of slipstream velocity. Typically, the axial velocity is greater than the forward speed of the ship in the outer portion of the slipstream and less than ship speed near the axis of rotation, as shown in Figure (18). The axial kinetic-energy loss would be reduced if the axial velocity was somehow increased near the axis of rotation, permitting a lower velocity in the outer region.

The second loss mechanism arises because the pressure must be lower than the ambient pressure across the entire downstream face of the slipstream. This reduction in static pressure across the slipstream is a result of the swirl in the slipstream. The static pressure is equal to the ambient pressure at its outer boundary and decreases continuously to a minimum at the axis of rotation. The radial equilibrium equation can be used in conjunction with the swirl distribution to obtain the static
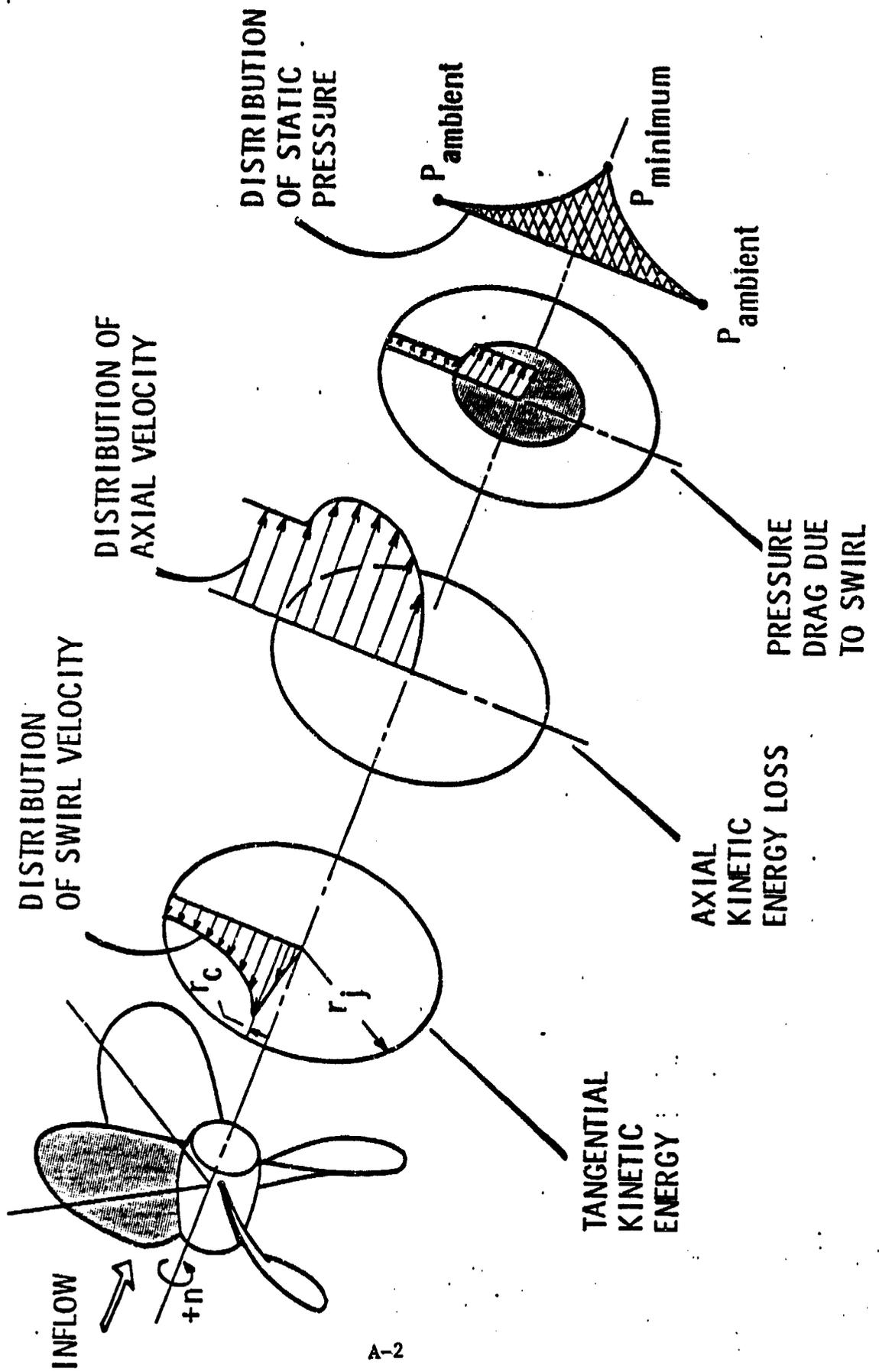
Figure 18. Schematic of Slipstream Swirl Losses

pressure distribution across the downstream face of the slipstream. The radial static pressure distribution can then be applied to derive the axial force on an annular increment of the slipstream. The increments of force can be summed over the entire slipstream to obtain the axial force resulting from the static pressure distribution caused by the slipstream swirl. This force acts to reduce the thrust of the propeller; the low pressure regions near the axis of rotation can be envisioned as a suction or drag force that reduces the propeller thrust.

Figure (19) shows how the lower-than-ambient pressure across the slipstream reduces the thrust. Consider a control volume around a propeller and the momentum flux as well as the pressure acting on the control volume. Applying the radial equilibrium equation with swirl in the slipstream, the static pressure $p_1$ is less than the ambient pressure $p_\infty$ across the downstream face of the slipstream. The energy added per unit mass flow $\Delta(UV_0/g)$ is the same in both cases; however, for a given shaft power, the thrust produced by the propeller is reduced if there is swirl in the slipstream.

With an analytical model of a propeller and the slipstream energy losses [1] it is possible to predict the magnitude of each of the energy losses as a function of propeller thrust coefficient, advance ratio, and diameter or ingested-mass flow.

The technical basis upon which predictions of the propulsor geometry and powering performance are performed is detailed in [1] and [2], however the basic physical description of the loss mechanisms associated with each are as discussed in the following section.

In summary if some means of counterswirl were applied such as counterrotating propellers or stationary vane systems to eliminate slipstream swirl then improvements in efficiency could be achieved. Smaller diameter propellers also result when some means of counterswirl is employed.
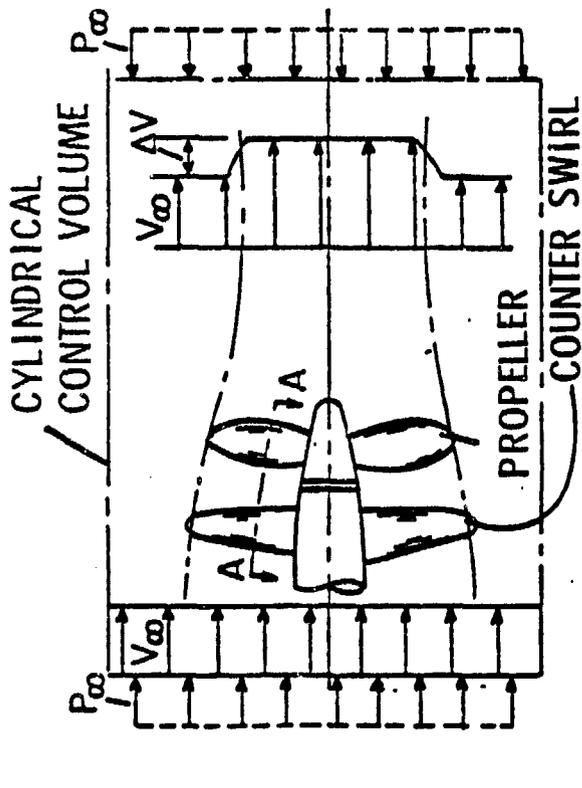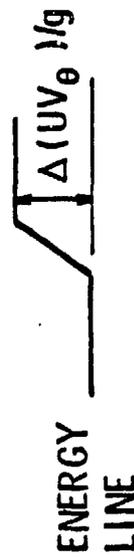
A-3
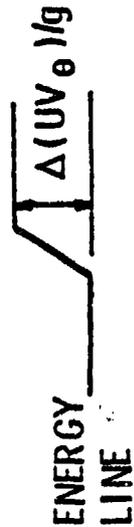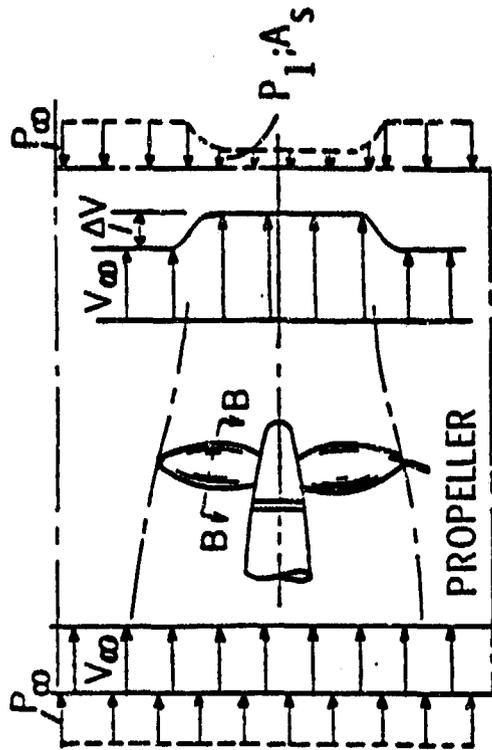
Figure 19. Control Volume Analysis Indicating How Reduced Pressure in Slipstream Reduces Thrust

A-4

The magnitude of the efficiency gain and decrease in propeller diameter becomes greater as lower shaft speeds or higher advance ratio units are considered.

## Preliminary Design Analysis

The following discussion outlines preliminary design analysis employed and the dependence of propulsor performance and geometry on the selected propulsor ingested mass flow. It is a __simplified__ and __condensed__ description of the computer coded analysis which is employed. It presents the basic concepts and provides a physical insight for those with technical backgrounds outside the area of propulsor design. A block diagram of the overall design exercise is outlined in Figure (20). If a more detailed description of the design is desired, References [1,2,3] are suggested.

Assuming the static pressure in the slipstream upstream and downstream of the propulsor are equal to ambient, the net thrust generated by a propulsor, with no slipstream swirl, can be expressed as;

$$C_T = \frac{Thrust}{\rho \frac{V_\infty^2}{2} A_B} = 2 \left( \frac{\rho \, Q}{\rho \, V_\infty \, A_B} \right) \frac{\overline{\Delta V}}{V_\infty} = 2 \, C_m \frac{\overline{\Delta V}}{V_\infty} \tag{1a}$$

where $\overline{\Delta V}/V_\infty$ is the mass averaged nondimensional increase in axial velocity and $C_m$ the mass flow coefficient. Note that this thrust is that which is reacted on to the vehicle; the algebraic sum of the rotor, shroud and stator thrusts. The quantity $A_B$ is a reference projected frontal area such as the propeller disc area. In this form it is apparent that a given thrust coefficient is the product of the mass flowrate coefficient ($C_m$) through the propulsor and the change in axial velocity that the flow experiences.

## DESIGN PROCEDURE

```
┌─────────────────┐      ┌─────────────────┐      ┌─────────────────┐
│  PRELIMINARY    │      │  FLOW-FIELD     │      │  BLADE-SHAPE    │
│  ANALYSIS       │ ───▶ │  DETERMINATION  │ ───▶ │  DETERMINATION  │
│  (1-D)          │      │  (AXISYMMETRIC) │      │                 │
└─────────────────┘      └─────────────────┘      └─────────────────┘
```

```
┌─────────────────────┐
│  BLADE SPECIFICATION│
└─────────────────────┘
```

**PRELIMINARY ANALYSIS (1-D)**

SELECTION OF PROPULSOR

INPUT:

BOUNDARY-LAYER PROFILE

ADVANCE RATIO

VEHICLE DRAG

OUTPUT:

TYPE OF PROPULSOR

EFFICIENCY

SIZE

CAVITATION & NOISE

**FLOW-FIELD DETERMINATION (AXISYMMETRIC)**

STREAMLINE CURVATURE PROGRAM WITH SPECIFIED SPAN & CHORDWISE BLADE LOADING

OUTPUT:

VELOCITY & ENERGY DISTRIBUTION THROUGH PROPULSOR

**BLADE-SHAPE DETERMINATION**

MEAN-STREAMLINE METHOD

INPUT:

SPACE/CHORD RATIO

BLADE NUMBER

THICKNESS DISTRIBUTION

OUTPUT:

BLADE SECTION DATA

CAVITATION PERFORMANCE

SECTION STACK-UP (SKEW)

STRESS CALCULATION

**BLADE SPECIFICATION**

LOFTING PROCEDURE USES 3-D CURVE FIT TO SPECIFY BLADE SECTIONS

A-6

Figure 20. Block Diagram of Design Exercise

It is assumed that the drag or resistance of the ship as a function of speed is known from towing tank tests or empirical based predictions. With these values of resistance, the change in velocity $\left(\frac{\Delta V}{V_\infty}\right)$ can be evaluated for the ship as a function of mass flow rate coefficient ($C_m$) using equation (1a). It is apparent from this relation that the axial velocity in the slipstream increases with decreasing mass flow. The impact of this on propulsive efficiency can be demonstrated by considering the definition of propulsive efficiency as being the effectiveness of the propulsor in converting the energy of the fluid passing through the propulsor into net thrust. This can be expressed as,

$$\eta_P = \frac{(\text{Thrust})(V_\infty)}{\text{Energy per Unit Time Placed in Fluid}} = \frac{(\rho Q \,\overline{\Delta V})(V_\infty)}{\rho \frac{Q}{2}(\overline{V}_j{}^2 - \overline{V}_1{}^2 + k\overline{V}_1{}^2)} \quad . \quad (2a)$$

The last term in the denominator of Equation (2a) represents an energy loss due to frictional effects and entrance losses to the duct if one is considered. The constant, k, has a nominal value of about 0.10 for ducted units.

$\overline{V}_j$ is the mass-averaged axial velocity in the downstream slipstream and is equal to the mass-averaged velocity upstream of the propulsor ($\overline{V}_1$) plus the change in axial velocity ($\Delta V$). On this basis $\overline{V}_j = \overline{V}_1 + \Delta \overline{V}$ and Equation (2a) reduces to,

$$\eta_P = \frac{1}{\dfrac{\overline{V}_1}{V_\infty} + \dfrac{1}{2}\dfrac{\Delta\overline{V}}{V_\infty} + \dfrac{k}{2}\left(\dfrac{\overline{V}_1}{V_\infty}\right)\left(\dfrac{\overline{V}_1}{\Delta\overline{V}}\right)} \tag{3a}$$

For a given mass flow rate, it is apparent from Equation (1a), the thrust developed is proportional to ($\Delta\overline{V}/V_\infty$). It is also evident from Equation (3a) that ingesting a given mass flow at an inflow velocity ($\overline{V}_1/V_\infty$) of reduced magnitude increases the propulsive efficiency and reduces the power required to produce this thrust. On this basis it is desirable to ingest low momentum boundary layer fluid from the hull, and accelerate, it rather than ingesting freestream fluid.

The mass averaged quantity $\overline{V}_1/V_\infty$ for a propulsor can be evaluated from a given velocity profile (either measured or computed) in the plane of the propeller, without the propeller present or operating, as a function of mass flow coefficient and the relation

$$C_m = \frac{\rho Q}{\rho \, V_\infty \, A_B} = 2 \int_{r_h/r_B}^{r/r_B} \left( \frac{V_1}{V_\infty} \right) \frac{r}{r_B} \; d \left( \frac{r}{r_B} \right) \qquad . \tag{4a}$$

The average velocity $\overline{V}_1/V_\infty$ for a given mass flow coefficient is then,

$$\frac{\overline{V}_1}{V_\infty} = \frac{C_m}{A_1/A_B} = \frac{C_m}{\displaystyle\int_{r_h/r_B}^{r/r_B} \left( \frac{r}{r_B} \right) \, d \left( \frac{r}{r_B} \right)} \qquad . \tag{5a}$$

These relationships also allow the average velocity upstream of the propulsor ($\overline{V}_1/V_\infty$) and the upstream area ($A_1/A_B$) to be plotted as a function of mass flow coefficient $C_m$.

The results so far have provided relationships indicating $\overline{V}_1/V_\infty$, $\Delta V/V_\infty$, and $\eta_p$ as a function of $C_m$. The initial information required is a velocity profile in the plane of the rotor without the rotor present, the rotor hub radius, body angle at this radius, and the effective horsepower or appended vehicle drag coefficient.

The power coefficient can now be obtained as a function of mass flow coefficient since:

$$C_p = \frac{\text{Shaft Power}}{\rho \, \dfrac{V_\infty^3}{2} \, A_B} = \frac{\text{Thrust } (V_\infty)}{\eta_p \, \eta_H \, \rho \, \dfrac{V_\infty^3}{2} \, A_B} = \frac{C_T}{\eta_p \, \eta_H} \tag{6a}$$

The hydraulic efficiency ($\eta_H$) represents the effectiveness of the blading to convert shaft energy into fluid energy. For a single stage axial flow pump, the value of $\eta_H$ nominally approaches 0.88. Equation (6a) permits the power

coefficient to be calculated as a function of mass flow coefficient. The power coefficient will achieve a minimum for some mass flow coefficient for the advance ratio considered. This is depicted schematically in Figure (21).

## Cavitation Performance as a Function of Mass Flow

The cavitation performance of the propulsor is dependent on the mass flow selected since this will effect propeller diameter. If a ducted propulsor is considered it is also strongly dependent on the amount of acceleration that is imparted to the fluid up to the plane of the rotor. This can be best described by considering Figure (22) where the static pressure associated with a streamline passing through the blade tip is considered. The static pressure ($p_2$), for a given mass flow, can be controlled by selecting the annular area enclosed by the duct at the rotor inlet. By this means, the pressure ($p_2$) could be greater, equal to, or smaller than ($p_\infty$). Therefore, if a duct geometry existed that diffused the flow from the duct inlet to the rotor inlet then the static pressure would be greater than ($p_\infty$). Conversely, if the duct was shaped to accelerate the flow from the duct inlet to the rotor plane the static pressure ($p_2$) would be less than ($p_\infty$). It is apparent for a given mass flow that selecting a 100 percent acceleration duct, results in a minimum in rotor tip diameter but could provide the poorest cavitation resistance since the static pressure immediately in front of the rotor is reduced.

The change in static pressure from upstream of the duct inlet to station (2) just upstream of the rotor can be written as:

$$p_\infty + \rho \frac{\overline{V_1}^2}{2} = p_2 + \rho \frac{\overline{V_2}^2}{2}$$
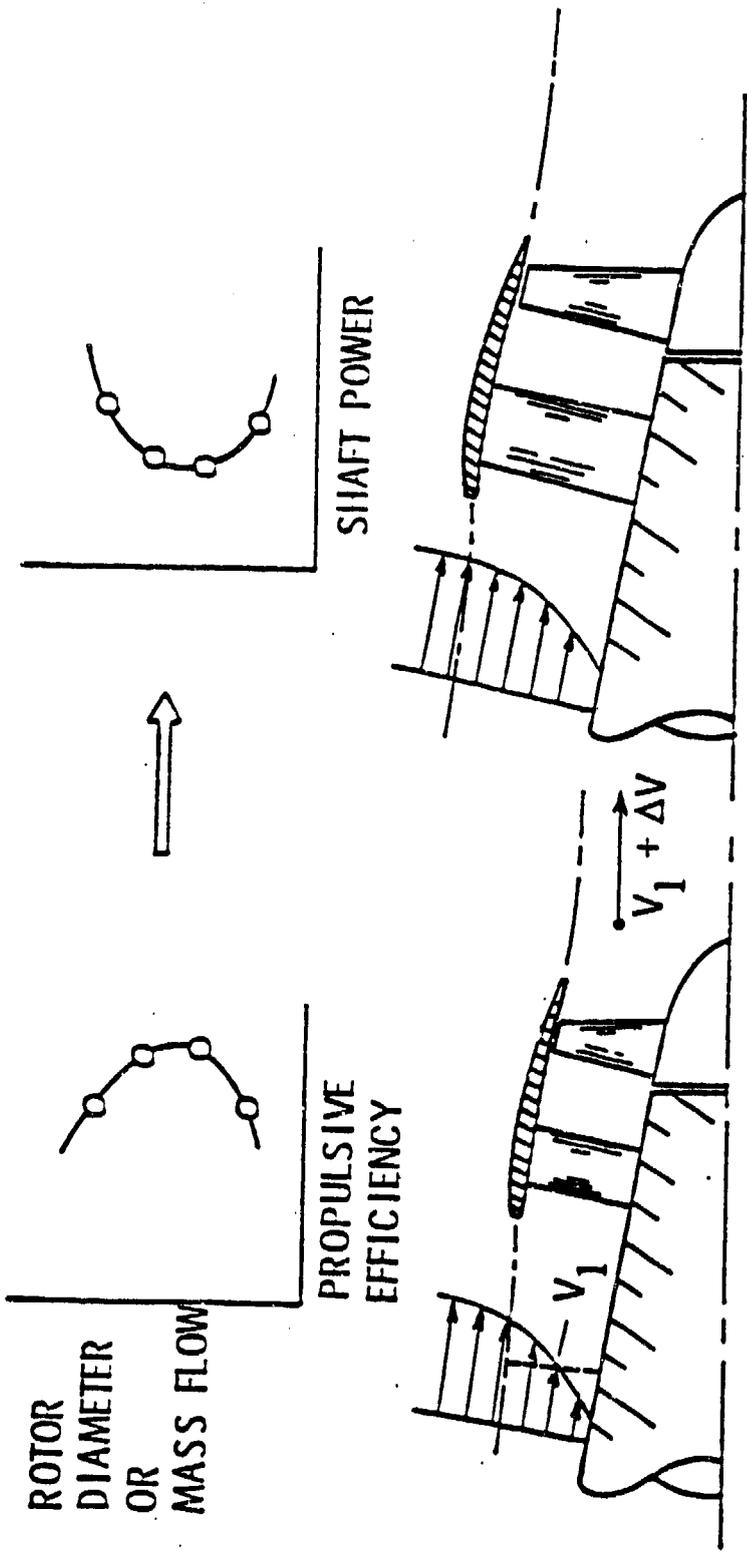
THRUST = $(\gamma/g)Q\ (\Delta V)$

HEAD = $f(\Delta V)$

SHAFT POWER = $(\gamma Q)(\text{HEAD})$

$(\gamma/g)Q$ = MASS FLOWRATE

$\Delta V$ = CHANGE IN AXIAL VELOCITY

Figure 21. Schematic of Shaft Power as a Function of Mass Flow
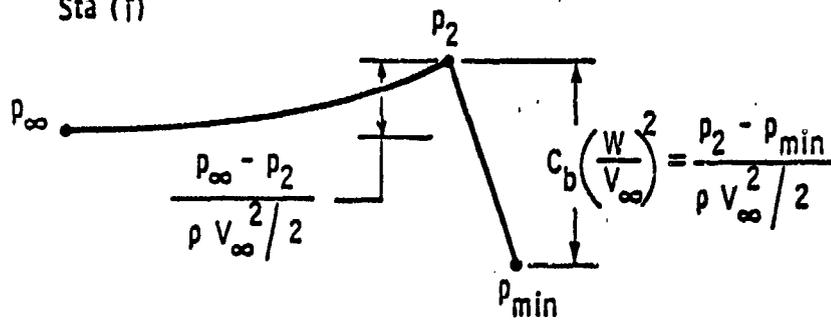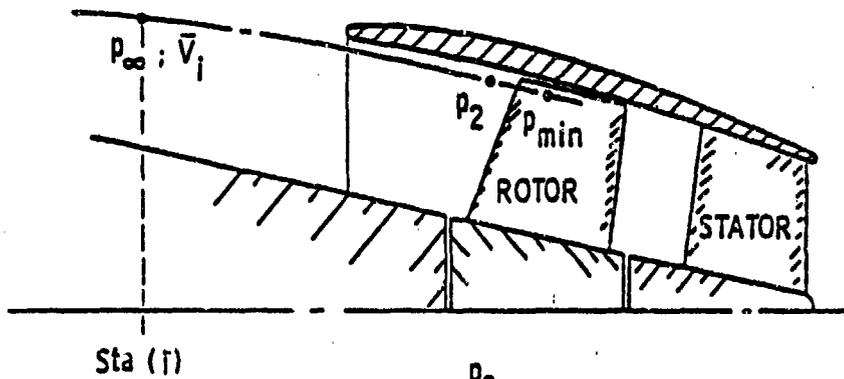
Figure 22.   Schematic of Static Pressure Distribution Along Tip
Streamline

or

$$\frac{p_\infty - p_2}{\rho \frac{V_\infty^2}{2}} = \left(\frac{\overline{V}_2}{V_\infty}\right)^2 - \left(\frac{\overline{V}_1}{V_\infty}\right)^2 \tag{7a}$$

The quantities $\overline{V}_2$ and $\overline{V}_1$ are the mass averaged meridional velocity and are composed of the axial and radial components in the flow. It had been previously discussed that $\overline{V}_2$ would be a maximum if all the change in axial velocity $(\Delta\overline{V}/V_\infty)$ was imparted to the fluid before it reached the rotor. In this case:

$$\frac{p_\infty - p_2}{\rho \frac{V_\infty^2}{2}} = \left(\frac{\overline{V}_1 + \Delta\overline{V}}{V_\infty}\right)^2 - \left(\frac{\overline{V}_1}{V_\infty}\right)^2 \quad . \tag{8a}$$

An additional change in static pressure occurs as the particle proceeds from station (2) to the minimum point of pressure on the blade. This is a function of the blade section geometry, the velocity relative to the blade section and the loading or lift coefficient of the blade. The blade pressure coefficient $(C_b)$ indicated in Figure (22) is about 1.0 for typical rotor blade sections on planing hulls. This quantity when multiplied by the nondimensional dynamic head of the flow relative to the blade tip approximates the static pressure drop from rotor inlet to the minimum pressure point on the blade. The cavitation index is the sum of the two described changes in static pressure indicated in Figure (22):

$$\sigma = \left(\frac{p_\infty - p_2}{\rho \frac{V_\infty^2}{2}}\right) + \left(\frac{p_2 - p_v}{\rho \frac{V_\infty^2}{2}}\right) \quad . \tag{9a}$$

A-12

This can be rearranged in terms of quantities already derived as,

$$\sigma = 2\left(\frac{\overline{V}_1}{V_\infty}\right)\left(\frac{\Delta\overline{V}}{V_\infty}\right)_R + \left(\frac{\Delta\overline{V}}{V_\infty}\right)^2_R + C_b\left[\left(\frac{\overline{V}_1}{V_\infty}\right)^2 + 2\left(\frac{\overline{V}_1}{V_\infty}\right)\left(\frac{\Delta\overline{V}}{V_\infty}\right)_R + \left(\frac{\Delta\overline{V}}{V_\infty}\right)^2_R + \right.$$

$$\left.\left(\frac{\pi}{J}\right)^2\left\{\frac{\dfrac{\overline{V}_1}{V_\infty}\dfrac{A_1}{A_B}}{\dfrac{\overline{V}_1}{V_\infty}+\left(\dfrac{\Delta\overline{V}}{V_\infty}\right)_R}+\left(\frac{r_h}{r_B}\right)^2\right\}\right] \qquad \text{(10a)}$$

The cavitation index can then be evaluated as a function of <u>mass flow coefficient</u> using Equation (10a) by inserting some fractional value of the total $(\Delta\overline{V}/V_\infty)$ indicated in Figure (4) for $(\Delta\overline{V}/V_\infty)_R$. In the programmed analysis there are three values for $(\Delta\overline{V}/V_\infty)_R$ corresponding to 0%, 50% and 100% of the total $(\overline{\Delta V}/V_\infty)$ occurring at the inlet plane to the rotor. The 50% represents that value associated with either the standard propeller or reaction fin unit.

## Rotor Tip Diameter as a Function of Mass Flow and Acceleration

The term in brackets on the far right of Equation (10a) is the square of the rotor tip diameter and can therefore be determined for each degree of acceleration as

$$\frac{r_t}{r_B} = \left[\frac{\dfrac{\overline{V}_1}{V_\infty}\dfrac{A_1}{A_B}}{\dfrac{\overline{V}_1}{V_\infty}+\left(\dfrac{\Delta\overline{V}}{V_\infty}\right)_R}+\left(\frac{r_h}{r_B}\right)^2\right]^{1/2} \qquad \text{(11a)}$$

This relation can be evaluated for any selected degree of acceleration as a function of mass flow coefficient. If a mass flow coefficient associated with a minimum in required shaft power is selected for a range of design advance ratios, the tip radius for a given propulsor can be evaluated by equation (11a).

A preliminary design analysis exists for the standard propeller and reaction-fin propulsor which is similar to that of the ducted propulsor. The primary difference being that for a selected mass flow coefficient or rotor diameter, the degree of acceleration up to the plane of the rotor, can not be controlled for the propeller and reaction-fin propulsor. Nominally, the change in axial velocity from far upstream to the plane of the rotor for these units would be about one-half the total change in axial velocity required to provide the necessary thrust. This would approach the 50 percent acceleration ratio case specified for the ducted propulsor.

A primary difference between the standard propeller and the reaction-fin propulsor is that the unit can be designed so all the counterswirl placed in the fluid by the stationary vanes is totally removed by the action of the rotor. Therefore, the reaction-fin propulsor experiences no slipstream swirl losses. This is in contrast to the standard propeller which does experience slipstream swirl losses.

The design of the non-axially symmetric stator is performed using the "parallel compressor theory" developed for gas turbine design. By this approach the flow is broken into separate quadrants and blade geometries designed to impart the desired flow deflection to that segment of flow being considered. The basic assumption is that the adjoining segment of flow is decoupled from the surrounding flow. In the present design, four separate quadrants were considered and resulted in the design of two separate blade geometries plus a trailing edge fairing attached to the bearing support strut. The use of this approach depends, to a high degree, on experimental data. The data base for such blade rows is limited and therefore the design is an approximation which can be strengthened with availability of more data.